EFFECT OF SULFATE CONTENT ON THE EVOLUTIVE FRACTURE BEHAVIOR AND PROPERTIES OF FIBER-REINFORCED CEMENTED PASTE BACKFILL

by

Aaron McAdie

A thesis
submitted to the Faculty of Graduate Studies in partial fulfillment of the requirements for the Degree of Master of Science
in Civil Engineering

Civil Engineering Supervisor

Dr. Liang Cui

Associate Professor – Dept. of Civil Engineering

Lakehead University Thunder Bay, Ontario August 2022

Author's Declaration Page

I hereby declare that I am the sole author of this thesis. This is a true copy of the thesis, including any required final revisions, as accepted by my examiners. I understand that my thesis may be made electronically available to the public.

Abstract

Backfilling technology is utilized globally to improve ore recovery, reduce mine-generated waste, and provide stability to underground voids. Cemented paste backfill (CPB), a mixture of mine tailings, cement binder, and mixing water is the desired method of backfilling. After filling the underground space (called a stope), CPB is required to provide ground resistance to the surrounding rock walls, be used as a roof for continued mining operations, or a floor for underground mine workers and equipment. A challenge to the use of CPB is the vast quantities of sulfide minerals such as pyrite and pyrrhotite containing irons present in the waste mine tailings. The sulfate anions generated from the oxidation of sulfide minerals not only interfere with the progression of cement hydration but also produce expansive hydration products, including gypsum and ettringite. As a result, the sulfate anions are able to change the microstructure and macroscale geomechanical behavior and material properties of the CPB materials. Therefore, it is of theoretical and practical importance to fully consider sulfate-induced evolution of mechanical behavior and properties of CPB materials. Moreover, the ability to extract ore up to the CPB pillar provides benefits to the profitability of the mine. However, mine stopes may reach enormous depths in excess of 100m into the earth. Therefore, the CPB is not only subject to the internal chemical effects of the sulfide minerals but also to the complex loading conditions present within the mine stope. As a type of brittle material, the failure processes in the CPB matrix are governed by crack propagation under field loading conditions. Such an event will not only reduce mine profitability but can also potentially be life-threatening to the underground workers. As a method to mitigate such risk, fiber reinforcement (FR-CPB) is a promising approach. Hence, it is crucial to systematically investigate the effect of sulfate solution on the tensile and fracture behavior and properties of fiber-reinforced CPB materials. The objective of this research is to experimentally study the evolution of fracture behavior and material properties of CPB and FR-CPB subjected to various levels of internal sulfate solution and loading (i.e., mode-I, mode-II, and mode-III) conditions at 3, 7, 28, and 90 days. Moreover, this study utilizes SEM technology to examine the microstructural evolution of the CPB and FR-CPB. The results obtained from this study determined that high levels of sulfate is detrimental to early-age (3-day) fracture behavior of CPB and FR-CPB. However, the continuous generation of expansive ettringite results in the formation of passive confinement locked in the hardened CPB matrix, which positively improves the development of fracture behavior (especially the post-peak pseudo-hardening behavior under mode-III loading) and properties from 7 days to

90 days. Moreover, there exists a discrepancy in the effect of sulfate content on fracture toughness under different loading conditions. It has been found that shear fracture toughness (K_{IIC} and K_{IIIC}) of FR-CPB displays a larger discrepancy with the changes in sulfate concentration relative to the evolution of tensile fracture toughness (K_{IC}). Furthermore, a strong correlation was found between stiffness and fracture toughness for the CPB and FR-CPB. Therefore, compared with fracture energy, fracture toughness can be chosen as a more appropriate fracture property for the engineering design of FR-CPB materials when the deformation control in the surrounding rock mass becomes the main concern in the design process. The obtained results provide an in-depth insight into the sulfate-induced evolution of fracture behavior and properties of FR-CPB under various loading conditions and thereby contribute to the safe design of FR-CPB materials.

Keywords: Backfill technology, CPB, FR-CPB, sulfate, fracture behavior, cementitious composites

Acknowledgments

I would like to express my sincerest gratitude to Dr. Liang Cui, my graduate research supervisor, who believed in my abilities and suggested I expand my knowledge and attempt this research task. His leadership and guidance throughout the entire process were outstanding, and his passion for and knowledge of civil engineering, laboratory research, and technical writing has become a source of inspiration for me.

Thank you to my family located throughout Canada (Richard, Margaret, and Alanna) for your kindness, support, and motivation during my graduate studies.

To the laboratory technicians Cory Hubbard and Morgan Ellis, thank you for all your support and teaching. The great advice and aid you provided throughout the challenges presented during the laboratory work undoubtedly enhanced my experience at Lakehead. To Brett Holmberg, my friend and fellow master's student colleague, thank you for sharing in all the ups and downs. The knowledge and discussion shared between fellow students is an aspect of the study that provides depth few other elements of university study can. The working relationship and friendship we have established is one I can only hope will continue well into the future.

To my thesis examiners, Dr. Baoqiang Liao and Dr. Jian Deng, thank you for taking your time and consideration of my work. The suggestions and insight provided by you both were extremely valuable and greatly improved the quality of my research.

Table of Contents

List of Tables

List of Equations

List of Figures

List of Abbreviations

CPB	Cemented Paste Backfill
FR-CPB	Fiber-Reinforced Cemented Paste Backfill
UCS	Unconfined Compressive Strength (kPa)
Cc	Cement Content (%)
w/c	Water to Cement Ratio
SEM	Scanning Electron Microscopy
XRD	X-Ray Diffraction
SCB	Semicircular Bend
ENDB	End Notch Disk Bend
LVDT	Linear Variable Differential Transformer
SB-DM	Strength-Based Design Method
TGA	Thermogravimetric Analysis
MIP	Mercury Intrusion Porosimetry
FA	Fly Ash
SF	Silica Fume
PC	Portland Cement
PPM	Parts Per Million

Nomenclature

Roman

P	Maximum Force (N)
D	Diameter of sample (m)
t	Thickness of sample (m)

B	Thickness of sample (m)
S	Distance between load frame support bars (m)
W	Width of sample (m)
a	Notch length (m)
K_{IC}	Mode-I Fracture Toughness (kPa·m$^{1/2}$)
K_{IIC}	Mode-II Fracture Toughness (kPa·m$^{1/2}$)
K_{IIIC}	Mode-III Fracture Toughness (kPa·m$^{1/2}$)
Y_I	Normalized stress intensity factor for mode-I
Y_{II}	Normalized stress intensity factor for mode-II
Y_{III}	Normalized stress intensity factor for mode-III
V	Volume of sample (cm^3)
M_c	Mass of wax coated sample (g)
M_t	Mass of sample (g)
M_{sub}	Mass of submerged wax coated sample (g)
w	gravimetric moisture content (%)
Wc	Work to crack initiation (Nmm)
Wf	Work of fiber bridging (Nmm)
E	Elastic modulus (kPa)
E_{50}	Secant modulus (kPa)
c	Cohesion (kPa)

Greek

σ	Normal stress (kPa)

τ	Shear stress (kPa)
φ	Internal angle of friction (°)
ε	Strain (mm/mm)

Chapter 1 Introduction

1.1 Background

Once the target mineral has been extracted from underground, the remaining space (stope) must be filled in using a process known as backfilling. Cement paste backfill (CPB) is a mixture of approximately 85% waste mine tailings, up to 9% binder, and mixing water and is used extensively in the backfilling process. The use of this novel technology possesses a number of advantages. Firstly, it reduces the potential for environmental contamination that may occur due to surface storage of the waste mine tailings (Rong et al., 2017). Tailings containing large quantities of sulfide minerals generate acid mine drainage (AMD) (Ethier et al., 2018; Jafari et al., 2021), which may leach through the containment barrier of the tailings pond. A surface breach of the tailings pond releasing AMD is also a risk. Placement of the tailings in solid form in the underground stope reduces the possibility of the two aforementioned scenarios from occurring. Secondly, there is a reduction in cost associated with the use of CPB technology over other methods of backfilling, such as the use of traditional cement concrete. Not only does the CPB reduce the size of the tailings pond providing economic benefit, but it also uses a very low mass of cement binder. As the cement binder in traditional concrete is around 20% when compared to CPBs 3-7%, there is a lower usage of the binder. Typically, the binder is one of the most expensive components of the mining operation. The use of CPB also provides stability benefits over other methods of backfill. Loosely placed rock backfill must be contained by surrounding rock walls. Therefore, there is a loss of profit associated with this method as there is no way to mine directly up to the filled stope to obtain the target mineral. Doing so would release the unstable rock fill, potentially endangering the lives of the underground workers. As CPB is a solid material, the adjacent pillars may be mined up to the surface of the CPB body. Additionally, CPB may be used as a roof in the underhand cut and fill method or used as a floor for mining equipment and workers.

As CPB must provide support to the surrounding rock mass (Cui & Fall, 2019; Fu et al., 2016; Yilmaz, 2018), it is commonly subjected to compressive loading. It is for this reason that a strength-based design method (SB-DM) has been adopted as a method of backfill design. Therefore, the unconfined compressive strength (UCS) is of vital importance and commonly utilized when considering the SB-DM of CPB technology. The vertical stress of the CPB mass is

typically predicted through analysis. From this analysis, the required strength of the CPB is determined in relation to a factor of safety (FS), typically in the range of 1.5-2.5. Once the required strength is determined, a mix design of the CPB is developed that is able to provide the required strength. Extensive studies have been conducted to investigate the UCS of CPB technology, providing significant insight into the mechanical behavior of the CPB when subjected to compressive loading. However, it is essential to note that CPB may be placed up to 100m or more in-depth beneath the ground. Once cured, it is subjected to complex loading conditions from the surrounding ore body and from any forces induced by continued mining operation (i.e., blasting or equipment usage). As CPB is a type of brittle material, this poses a challenge to the usage of CPB. The brittle nature of the CPB, combined with the complex loading conditions, creates a risk to the usage of CPB as the probability of catastrophic failure of the CPB body is extremely high. The build-up of strain energy may be released without warning reducing the progress of mining production and potentially injuring or killing any workers present. It is for this reason, there is a need to find methods to further improve the implementation of CPB technology and potentially reduce the risk of catastrophic failure of the material. Therefore, in this regard, the fiber reinforcement technique offers a promising approach. Figure 1.1 is a diagram showing the placement of CPB and the loading that may be placed on the backfill material once poured into the underground stope.

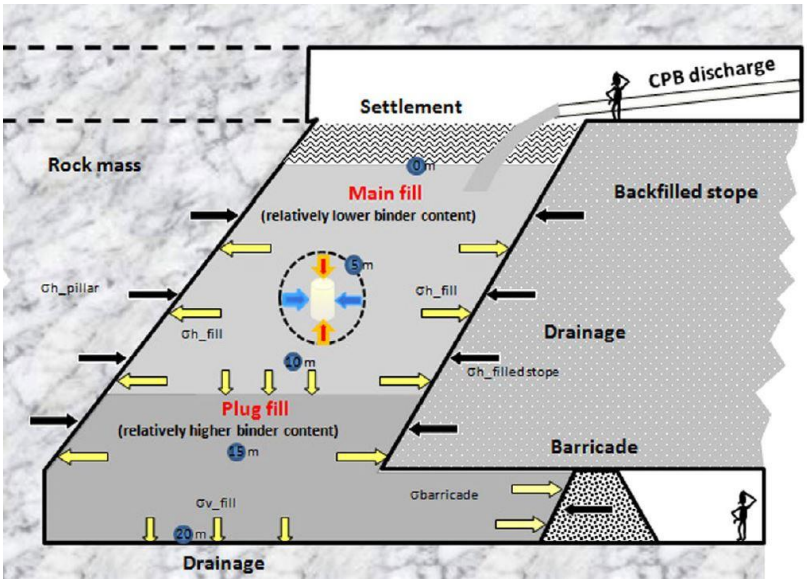

Figure 1.1. Stope diagram and complex loading conditions present in underground mining (Yilmaz, 2018).

Fiber-reinforced CPB (FR-CPB) is an improvement to conventional CPB. As the strain energy releases from the CPB due to external loading, there is a complete release along fracture planes within the body of the CPB. Namely, once the interparticle matrix has broken, there is no longer a method to keep the CPB pillar intact. However, with the addition of fibers in the CPB matrix, the post-peak load resistance is capable for the CPB. This method adds some ductility to the CPB body. Therefore, if there is subsidence or release, some additional load is required to fracture the CPB completely. Thus, the risk of catastrophic failure is significantly reduced, and the potential for improved ground monitoring of the CPB within the stope is increased.

1.2 Problem statement

Previous studies conducted have focused on the conventional geomechanical behaviors, including compressive, tensile, and shear behaviors of CPB materials (Aldhafeeri & Fall, 2017; Fang et al., 2020; Fang & Fall, 2019; Guo et al., 2020; Li & Fall, 2016, 2018; Nasir & Fall, 2008). However, as a type of cementitious material, the failure process is featured with the crack initiation and propagation in the CPB and FR-CPB matrix. Moreover, the in-situ complex loading conditions, especially the polyaxial loading conditions present in underground mining, result in the simultaneous development of tensile and shear cracks in CPB mass (Xiu et al., 2021). Therefore, the systematic investigation of fracture behavior and properties of FR-CPB under mode-I (tensile), mode-II (in-plane shear), and mode-III (out-of-plane shear) provide in-depth insight into the mechanical behavior and performance of cementitous materials and thus contributes to its successful engineering implementation of fiber reinforcement in underground mine backfill operations.

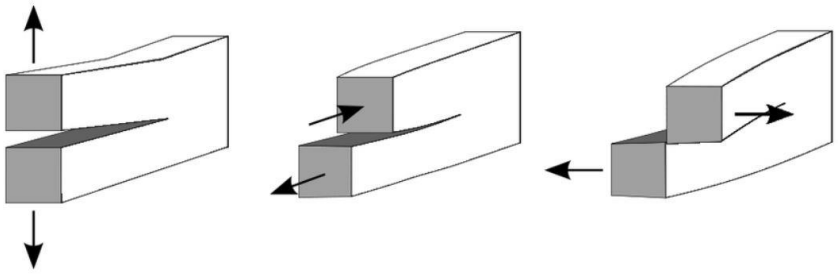

Figure 1.2. Fracture behavior modes I, II, and III (Vyazmensky, 2008).

Sulfide minerals are abundant within the crust of the earth and therefore are a very common product to encounter when extracting target ore. The sulfide minerals, when exposed to oxygen

and water, produce sulfate within the mine tailings (Liu et al., 2019). The sulfate reacts with products contained within the cement binder utilized to create the CPB or FR-CPB. The products formed due to these chemical reactions, namely gypsum and ettringite, are expansive in nature and rapidly form within the pore spaces of the CPB. This expansive formation at the microscale level can affect the macroscale performance of the CPB in various ways. There is some evidence to suggest that expansive phase production can actually enhance the microstructure of the CPB matrix resulting in improved mechanical behavior and material properties. However, further evidence suggests continued development of the expansive phases can result in microcracking pressure within the CPB and form micro fissures within the CPB matrix. In turn, these microcracks produced by the excess sulfate content have a detrimental effect on the CPB performance and material properties. The exact details regarding the chemical reactions and studies regarding the effect of sulfate on the behavior and material properties of the CPB will be addressed further in greater detail in Chapter 2, Literature review.

Currently, no studies have been designed and conducted to systematically investigate the effect of sulfate content on fracture behavior of CPB/FR-CPB, which significantly affects the thorough understanding of the failure process in CPB materials and thus the safe design of CPB/FR-CPB technology. To address this research gap, a comprehensive experimental testing program is developed through this thesis study to investigate the effect of sulfate content on the evolutive mode-I, mode-II, and mode-III fracture behaviors and properties of CPB/FR-CPB at various curing times. The obtained results can significantly improve the understanding of the engineering behavior of sulfate-rich CPB/FR-CPB materials and thus promotes its successful application in underground mining backfill operations.

1.3 Research methodologies

In order to systematically investigate the effect of sulfate content on the fracture behavior and properties of CPB and FR-CPB, extensive laboratory and mathematical analyses were conducted. Each component of the study to achieve this goal is listed as follows:

1. Develop base knowledge and understanding of the effect of internal sulfate on the mechanical behavior and material properties through a detailed literature review of current knowledge on the applicable subject matter. Then, a research gap is identified in relation to the current conventional knowledge.

2. Prepare a series of CPB and FR-CPB cylindrical molds to thoroughly conduct experimental testing on the mode-I, mode-II, and mode-III fracture behavior of the CPB and FR-CPB.
3. Utilize semicircular bend (SCB) and end notch disk bend (ENDB) testing to observe the fracture of the CPB and FR-CPB at various sulfate contents and curing times.
4. Analyze the obtained fracture behavior data to further investigate the effect sulfate concentration has on the fracture toughness, stiffness, work to crack initiation, and work of fiber bridging material properties of the CPB and FR-CPB.
5. Utilize ASTM D7263-21 method A to analyze the dry density of the CPB and FR-CPB to determine the effect internal sulfate has on the microstructural density of the material.
6. Conduct scanning electron microscope (SEM) observation on the microstructure of the CPB and FR-CPB to observe the formation of the hydration products and expansive phases within the bulk matrix. The microstructure changes, in turn, will provide clarity as to the changes to mechanical behavior and material properties of the CPB and FR-CPB.

1.4 Thesis organization

The presentation of the research work conducted throughout this study is divided into five chapters. Chapter 1 introduces the rudimentary information regarding the CPB and FR-CPB technology as well as introduces the problem statement, research methodologies, and thesis organization. Chapter 2 provides the pertinent information reviewed in the literature review stage of the research. The information covered in this section reviews the origin and generation of sulfate in waste mine tailings, the chemical reactions occurring within the CPB body, and the current knowledge on mechanical behavior and material property changes as a result of the internal sulfate content. Chapter 3 details the material preparation and experimental equipment used to conduct the research. The detailed procedures utilized to analyze the material properties are also outlined in this chapter. Chapter 4 is a detailed breakdown of the results obtained from the research. The chapter first outlines the mode-I, mode-II, and mode-III fracture behavior results obtained. Then, a discussion on the evolution of the material properties is presented, followed by an additional sensitivity analysis of the results. Finally, Chapter 5 summarizes the previous four chapters and draws conclusions from the conducted research work. From the conclusions, a set of recommendations is made regarding possible future work to improve the understanding of the effect of sulfate content on CPB and FR-CPB.

Chapter 2 Literature review

2.1 Introduction

Cement paste backfill (CPB), a material mixture of tailings, binder, and water, is poured into complex underground structures referred to as stopes (Cui & Fall, 2018). CPB is a widely used backfilling technology in the mining industry for the disposal of mine waste tailings. This technology is used to provide long-term economic and environmental benefits to the mining industry. Since the failure of CPB within a mine may result in a financial loss (Li & Fall, 2018) and possible loss of life, it is necessary to implement a proper design method and maintain the mechanical stability of CPB mass during its service life (Fall et al., 2007; Liu et al., 2019). In this regard, the strength-based design method (SB-DM) has been widely adopted in underground mine fills (Libos & Cui, 2020a). As a secondary ground support means, CPB mass is commonly subjected to the compressive loadings from rock roofs (Libos & Cui, 2020b). Correspondingly, the unconfined compressive strength (UCS) is commonly utilized in the SB-DM. During the design phase, the vertical stress near the stope base is first estimated through analytical methods or numerical methods. Then, the design strength (required strength) can be back-calculated by the product of pre-specified factor of safety (Fs=1.5 to 2.5) and the estimated vertical stress (Wang et al., 2020). After that, the obtained design strength will be used to determine the mix proportion of CPB for the target stope. Correspondingly, the investigation of the UCS and associated influential factors have attracted great attention in the field of mine backfills. Based on previous studies (Orejarena & Fall, 2010; Rong et al., 2017), it has been found the sulfate attack plays a critical role in the evolution of UCS and the mechanical stability of CPB structures. Specifically, due to wide existence of sulfide minerals high sulfate concentration is typically found in mine waste tailings. Sulfide (e.g., FeS_2) oxidizes in the tailings to produce sulfate (SO_4^{2-}) ions. The following reaction represents the oxidation of sulfide into sulfate:

$$2FeS_2 + 7O_2 + 2H = 2Fe^{2+} + 4SO_4^{2-} + 4H^+ \quad (2.1)$$

Since molecular formulas for reactants and products involved in sulfate attack can be long and cumbersome to continuously write. Cement Chemist Notation (CCN) is used to simplify the writing of the reactions in the present paper. The acronyms are used to identify each constituent used in cement chemical reactions: C=CaO, S=SiO_2, A=Al_2O_3, $\underline{S}$=SO_3, H=H_2O, F=Fe_2O_3. As the

sulfate ions originate from the CPB mixture this is considered an internal sulfate attack. A series of complex chemical reactions occur between the cement paste binder and water. Typically, Portland cement is used as the binder material (Li and Fall, 2018). Portland cement is comprised of four main constituents: tricalcium aluminate (C_3A), tricalcium silicate (C_3S), dicalcium silicate (C_2S) and tetracalcium aluminoferrite (C_4AF). A small amount of gypsum ($C\underline{S}H_2$) may also be included in the Portland cement to control the setting characteristics of the CPB (Liu et al., 2019). The series of hydration reactions occurring within the CPB can be generalized as follows:

$$2C_3S + 6H = C_3S_2H_3 + 3CH \tag{2.2}$$

$$2C_2S + 4H = C_3S_2H_3 + CH$$

$$C_3A + 6H = C_3AH_6$$

$$C_4AF + 7H = C_3AH_6 + CFH$$

Hydration of the cementitious materials creates a matrix structure of calcium-silicate-hydroxides (CSH) that dominates the short and long-term CPB strength (Liu et al., 2019). However, the C_3A reacts with sulfate ions and produces an additional product, ettringite ($C_6A\underline{S}H_{32}$), represented in the following equation:

$$C_3A + C_3\underline{S}H_2 + 26H = C_6A\underline{S}_3H_{32} \tag{2.3}$$

As an expansive phase, ettringite possesses a long needle-like hexagonal crystalline structure. When there exist adequate sulfate ions, the C_3A will be completely consumed to form the ettringite. Present studies (Rong et al., 2017; Xu et al., 2020) on the compressive strength of CPB indicate that expansive phases may refine the pore space and that there is an optimum sulfate content and curing time that can provide the maximum strength to the CPB. However, the literature indicates that above this optimum sulfate content, the ultimate compressive strength (UCS) will deteriorate over time (Neto et al., 2021). With the continuous formation of high volume ettringite in the pore spaces, cracking pressure is produced, which may cause microcracking in the CSH matrix and material degradation at the macroscale (Liu et al., 2019).

Since the material-strength-based design method is widely utilized in the design of CPB, there is a need to understand the link between the microcracking of the hardened CPB due to sulfate attack and the mechanical properties of the CPB. In order to evaluate the effects of sulfate attack on the

hardened CPB materials, understanding how microcracking develops to produce large-scale damage to the hardened CPB mass is required. Therefore, the objective of this literature review is to evaluate previous work on the effects of sulfate attack on the microstructure changes and mechanical response of CPB at the macroscale.

2.2 Microstructure changes in CPB under sulfate attack

At the beginning of early-age development (<28 days) CPB is prepared by mixing mine tailings, Portland cement, and water. From the initial mixing stage, a series of reactions begins to occur, which leads to the hardening process in CPB and contributes to strength development. Alite (C_3S) and belite (C_2S) are hydrated to form CSH and CH at different reaction rates. Since the hydration process associated with C_3S is rapid, the C_3S-induced CSH and CH are responsible for the early-age strength development. Correspondingly, C_2S-induced hydration products mainly contribute to the long-term material strength. It should be pointed out that the generated CSH accounts for more than 50% of hydration products and thus plays a dominant role in the strength formation of cementitious materials (Liu et al., 2019). However, when the mixture is high in sulfide-rich waste tailings, the oxidation of sulfide minerals occurs and results in the generation of sulfate solution in CPB. The free sulfate ions will further react with CH to produce gypsum. The gypsum continues to react with C_3A producing additional ettringite in the CPB. Over the development of CPB into advanced ages (≥28 days) excess sulfate ions produce large volumes of ettringite. To quantitatively or qualitatively evaluate the microstructure changes under sulfate attack, various techniques, including scanning electron microscopy (SEM), thermal gravimetric analysis (TGA), mercury intrusion porosimetry (MIP), and X-ray diffraction (XRD), have been widely adopted. The typical findings through each approach are summarized in the following subsections 2.3-2.6.

2.3 Scanning Electron Microscopy

SEM is used to visually observe material at the microscale. SEM observation involves scanning the surface of a material with a beam of electrons. The electrons provide information about the topography of the material surface under observation. The resolution achieved by SEM is in the micron to nano-scale range (Keneti & Sainsbury, 2018). Therefore, the advantage of using SEM observation is the images provide direct evidence for the generated hydration products, expansive

phases, and microstructure of the CPB matrix. The following SEM image shows the various cement hydration components and their morphology.

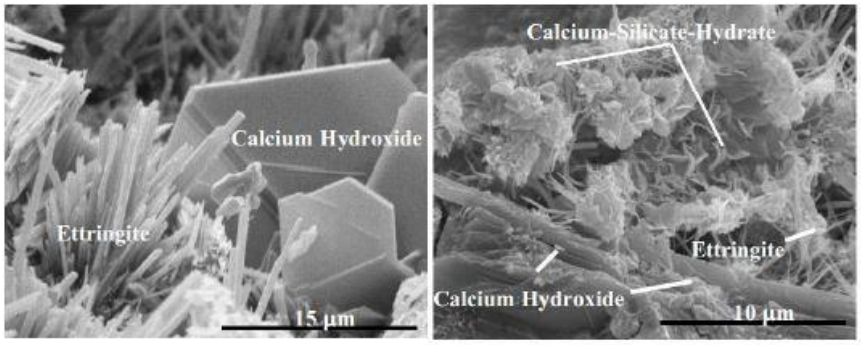

Figure 2.1. SEM image of cement hydration products (Shaikhon, 2015).

By analyzing SEM images of CPB, hydration products and expansive phases have been observed over the course of CPB development and discussed in the literature (Cihangir et al., 2015; Wang et al., 2020). For example, as shown in Figure 3 (Shaikhon, 2015), the SEM images taken from early development to long-term development all confirm the presence of gypsum and ettringite within the CPB. Consequently, the generated expansive phases considerably increase the pore space in the hardened matrix and thus cause the cracking pressure and associated microcracks in the porous matrix. Therefore, the SEM images offer valuable information about the hydration products and their effects on the matrix structure at the microscale. However, using SEM images alone will not confirm the exact volume of the expansive phases within the CPB. Therefore, although SEM can confirm the presence of gypsum and ettringite in a CPB sample under sulfate attack, the limitation of SEM is that it is qualitative and will not confirm the exact amount of ettringite formed due to excess sulfate ions. Due to SEM analysis being limited, it can be conducted in conjunction with energy dispersive x-ray spectroscopy (EDS, energy dispersive x-ray spectroscopy). EDS relies on an x-ray beam to excite the atoms within a material. The resultant signals from the excitations identify the atoms within the material. Each chemical compound provides a unique set of peaks on the electromagnetic emission spectrum, and thus, EDS analysis can be used to identify the changes in cement hydration products with curing time. For example, Wang et al. (2020) utilized SEM observation as well as EDS analysis to investigate the microstructure of CPB at 30 days and 160 days under sulfate attack. The results show that additional expansive phases, including gypsum had formed at 160 days and confirmed expansive

phases had increased over time. The SEM and EDS results from that study are shown in Figure 2.2. Figure 2.2 (d) shows an increase in sulfur when compared to the 30 days (Figure 2.2 (b)), also indicating higher quantities of expansive phase formation. The authors also state, "the accumulative formation of gypsum leads to the destruction of the dense microstructure of CPB subjected to long-term sulfate attack" (Wang et al., 2020).

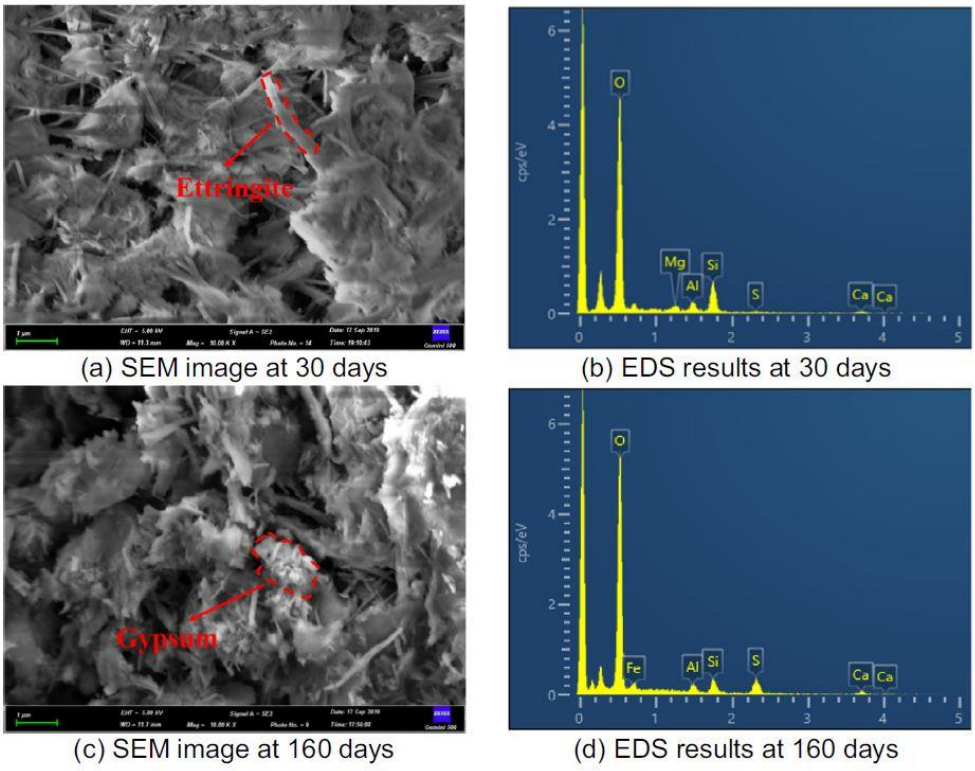

Figure 2.2. SEM and EDS of CPB conducted at 30 and 160 days (Wang et al., 2020).

2.4 Thermogravimetric Analysis

The second method to measure the volume of expansive phases within CPB is by thermogravimetric analysis (TGA). TGA measures the mass of the CPB sample as the temperature is increased. The increase in temperature and change in mass provides information as to the thermal decomposition of the CPB. Decomposition peaks occur when elements of the CPB decompose at their specified temperature. For example, Yan et al. (2020) found that gypsum and ettringite crystal water usually dehydrate at 100-160°C, and CH dehydrates at 400-500°C. The decomposition of calcium carbonate, as well as CH, occurs at 600-700°C. As the amount of expansive phase increases or decreases within the CPB sample depending on initial sulfate content, the

thermogravimetric analysis will show the corresponding changes in mass. Moreover, Yan et al., (2020) found that when sulfate content is relatively high (e.g., 25000ppm), more mass loss occurs in the 100-160°C range. Such mass change results from the dehydration temperature of gypsum and ettringite. This suggests that there are more expansive phase products in high sulfate samples when compared to samples with lower sulfate concentrations. Similar findings were found by Li and Fall (2018), where slag-CPB with 0, 5000, and 25000ppm sulfate contents were aged for 28 days before TG analysis was conducted. The results of the TG analysis can be seen below in Figure 2.3.

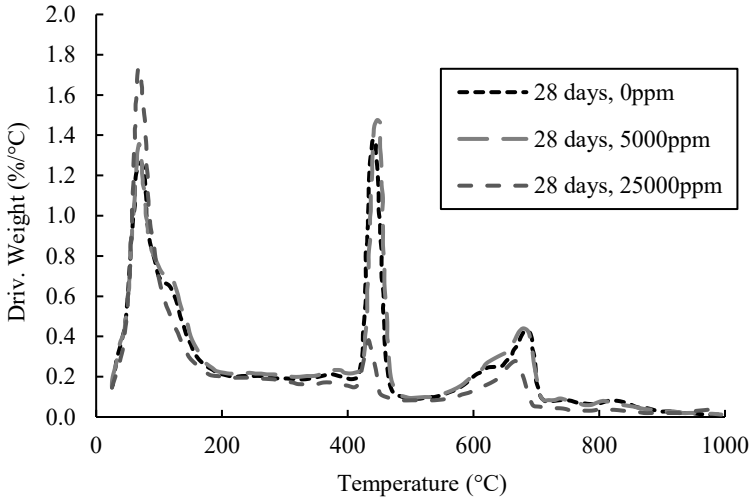

Figure 2.3. Dehydration of cement paste samples at 0, 5000, and 25000ppm sulfate content (Li & Fall, 2018).

2.5 Mercury Intrusion Porosimetry

Mercury intrusion porosimetry (MIP) is an analytical technique used to determine various aspects of a material such as pore diameter, pore volume, and pore structure by forcing mercury at pressure into the porous media (Gallé, 2001; Ma, 2014). As curing time elapses, there is a coarsening process of the pore structure within the CPB due to sulfate attack (Pokharel & Fall, 2013). As coarsening of pore structure is associated with increased porosity, data from the MIP analysis is able to quantitatively show how sulfate attack alters the microstructure of the CPB. The previous studies conducting MIP measurements found that the effect of sulfate attack on the porosity of CPB is twofold. First, during an early age, Rong et al. (2017) confirmed that total porosity, regardless of sulfate concentration, decreases from 7 to 28-day age (Figure 2.4). As the expansive phases continue to form, they fill the pore spaces of the CPB during this time.

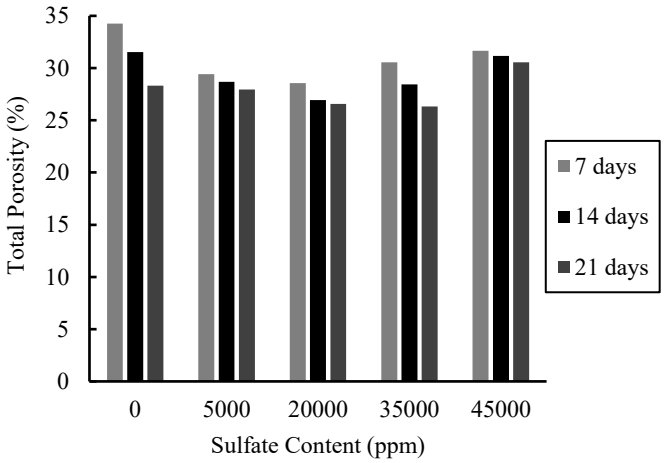

Figure 2.4. Total porosity of CPB with increasing sulfate concentration and curing times (Rong et al., 2017).

Second, at advanced ages, Aldhafeeri & Fall (2017) found that at around 150-days, the CPB samples under sulfate attack possessed a larger porosity which clearly indicates coarsening of the porous matrix within the CPB. The coarsening of pore structure can be quantitatively evaluated by the MIP measurements, which can be seen in Figure 2.5 (Aldhafeeri & Fall, 2017).

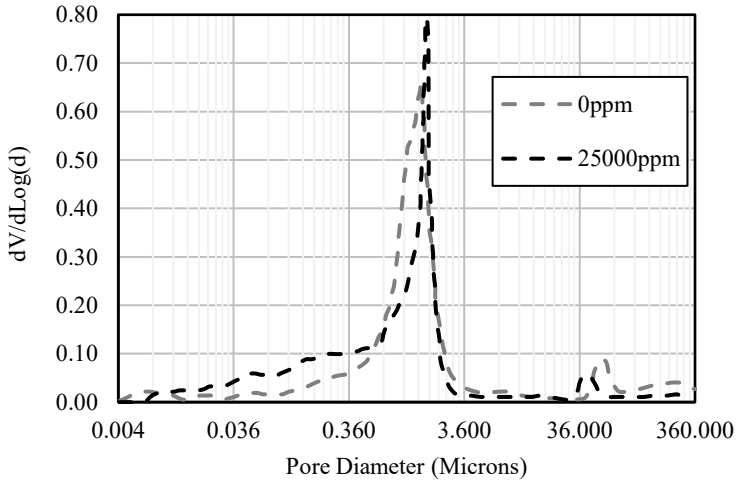

Figure 2.5. Pore diameter of PC-CPT with 0ppm and 25000ppm sulfate concentrations (Aldhafeeri & Fall, 2017).

2.6 X-Ray Diffraction

XRD is a useful technique because it enables the identification of major crystalline products in a cementitious material (Li et al., 2019). As CPB is composed of many components of crystalline morphology, XRD is an appropriate technique to determine the composition of the CPB. For instance, Li and Fall (2016) employed XRD analysis to determine the effect of sulfate attack on the microstructure of CPB at 3 days. Figure 2.6 shows the XRD results of 3-day CPB samples

indicate higher levels of ettringite were generated at higher sulfate concentration when compared to control samples with zero sulfate concentration. Additionally, very small amounts of gypsum were detected in each sample, suggesting that the formation of the early-age expansive phase is dominated by the generation of ettringite.

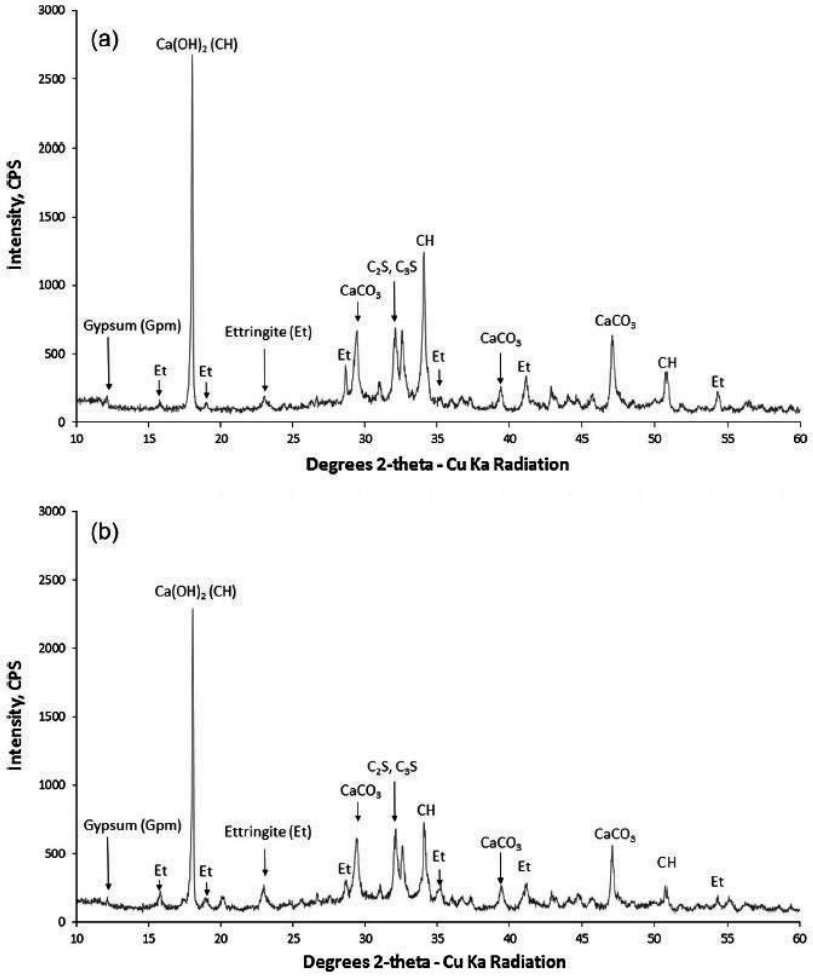

Figure 2.6. XRD analysis of CPB at 0ppm sulfate content (a) and 25000ppm sulfate content (b) at 3 days curing time (Li & Fall, 2016).

At advanced ages, Pokharel & Fall (2013) conducted XRD analysis on CPB samples aged for 90 days. It has been found that more expansive phases, including ettringite and gypsums, were formed in the CPB matrix as sulfate concentrations increased. Additionally, the XRD analysis clearly showed that more residual C_2S and C_3S were found in advanced-age CPB with the increase in sulfate concentration, which indicates the retardation or inhibitory effect of sulfate attack on the

formation of CSH. Consequently, the sulfate attack is able to further weaken the long-term material strength.

2.7 Mechanical behavior and properties of CPB under sulfate attack

The sulfate attack can yield distinct evolution of the microstructure of CPB from early to advanced ages. Correspondingly, such microstructure changes will eventually affect the mechanical behavior and properties at the macroscale. Therefore, the following sections aim to review the evolution of stress-strain response, including pre- and post-peak behaviors of CPB under sulfate attack. The associated transition between ductile and brittle behaviors of CPB will be discussed as well. Meanwhile, a detailed review of the effects of sulfate attack on the macroscale mechanical properties, including elastic modulus, UCS, and shear strength parameters (i.e., cohesion and angle of internal friction), will be conducted in Section 2.9. Apart from the evolutive characteristics of mechanical properties under sulfate attack, the engineering meaning of each mechanical property will also be discussed, which can contribute to the identification of the critical mechanical property for a particular engineering problem associated with CPB technology.

2.8 Compressive stress-strain behavior of CPB under sulfate attack

The microscale changes in the CPB due to sulfate attack will affect the macroscale engineering performance of the CPB. As the CPB is placed into underground stopes, the surrounding rock compresses the CPB mass. The induced stresses, in turn, produce deformation in the CPB. Understanding the evolutive stress-strain behavior of the CPB under sulfate attack will provide greater insight into the changes in the engineering performance of CPB mass. In this regard, the effect of sulfate attack on pre-and post-peak behavior at different curing stages must be evaluated.

From the literature, there is evidence that during early ages, the reaction products associated with sulfate ions can benefit the material strength and improve the stress-strain response (Fall & Benzaazoua, 2005; Li & Fall, 2018; Pokharel & Fall, 2013; Rong et al., 2017; Yan et al., 2020). Figure 2.7 shows how increased sulfate content affects the stress-strain behavior of CPB. The early age pre-peak behavior of each CPB sample can be seen. When sulfate content is increased, there is a more immediate stress response when compared to samples with lower sulfate content. This would indicate that increased sulfate content in the CPB provides increased ground support in the early-age periods. In early age development, the CPB samples with increased sulfate content

produce more expansive phases, which refine the pore structure. The pre-peak behavior in the stress-strain curve and the effect of the increased densification of the microstructure can be observed in Figure 2.7. The resultant stiffer CPB with higher sulfate content is able to provide more immediate ground support to the surrounding rocks at a given strain level and thus contribute to the mechanical stability of CPB mass during the early ages. For the post-peak behavior, there is a rapid loss in strength and a steep decline in axial stress as the strain continues to progress. Moreover, compared to control CPB without sulfate content, the change from a ductile to brittle behavior of the early-age CPB with increased sulfate content is evident in the post-peak stage.

Variations in brittle or ductile response can be explained by analyzing the shear behavior of the CPB. In CPB, the Portland cement content is low compared to other cementitious materials such as concrete. In soft cementitious materials, cohesion is relatively weak due to the low cement content. Friction resistance, by comparison, is a measure of the coefficient of friction between particle surfaces and is mobilized along the shear crack surfaces. In soft cementitious materials, the friction resistance dominates the shear strength relative to the cohesion. When crack failure propagates through the CPB matrix, the cohesion does not significantly affect the load carrying capacity of the material. Therefore, when CPB is subjected to compressive loading, there is a gradual release of strain energy which is evident by the ductile stress-strain response. Conversely, when brittle materials are subjected to compressive loading, there is a sudden release of strain energy. The sudden release of strain energy is evident by the sudden drop in axial stress in the post-peak stress-strain behavior. It is important to note that the increased material stiffness and subsequent brittle behavior in CPB with increased initial sulfate content are not due to an increase in cohesion of the CPB matrix. Current literature (Aldhafeeri & Fall, 2017; Pokharel & Fall, 2013) states that sulfate ions can actually inhibit the strength increasing hydration reactions within CPB. Rather, the increase seen when sulfate concentration is increased is due to a densification of the CPB mass due to the formation of expansive phases. There is an optimum time where the internal pores of the CPB are filled with gypsum and ettringite prior to the increase in internal stress due to crystal formation pressure and the resultant formation of internal cracks.

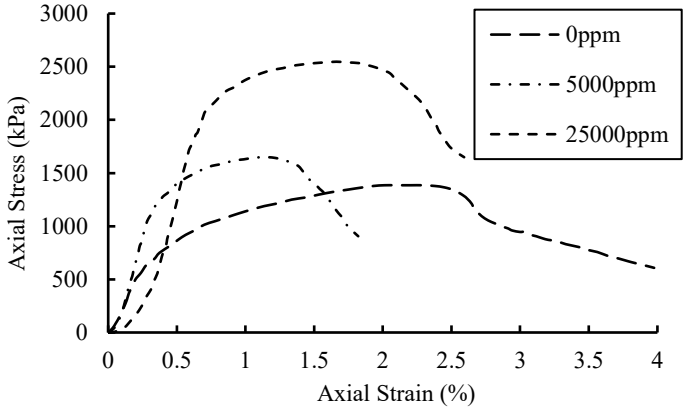

Figure 2.7. Stress-Strain behavior of CPB at 0, 5000, and 25000ppm sulfate concentration at 7 days (Yan et al., 2020).

When CPB transitions from early to advanced ages, the stress-strain behavior changes. The material may not show any signs of linear elasticity, and the peak stress may be lower compared to the counterparts with a less sulfate content. For example, Fall et al. (2007) studied the effect of sulfate content on the stress-strain behavior at 28 days. In this literature review, 28-days is defined as the cut-off time between the early and advanced stages of CPB development. The start of the advanced age effects of sulfate attack on the CPB can be observed in this study. Ettringite consumes water within the pore structure and swells (Liu et al., 2019). As expansive phase production continues in the CPB specimens with increased sulfate content, internal stress from the crystal generation can reach 200Mpa damaging the microstructure of the CPB (Li et al., 2018). Therefore, the CPB with lower sulfate content has an improved ability to provide ground support when evaluated at advanced ages. As sulfate content is increased, the increased expansive phase development over time coarsens the pore structure and induces cracking, causing strength deterioration (Fall & Samb, 2009; Ghirian & Fall, 2015).

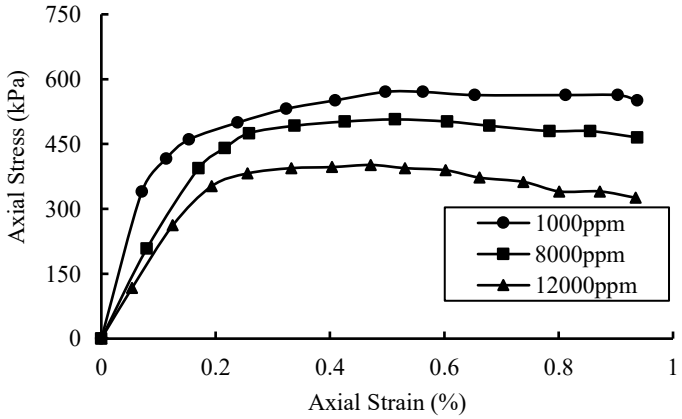

Figure 2.8. Effect of sulfate content on stress-strain behavior of CPB at 28 days (Fall et al., 2007).

2.9 Evolution of mechanical properties of CPB under sulfate attack

2.9.1 Unconfined Compressive Strength

UCS is commonly used in SB-DM of underground mine fill as the UCS corresponds to the peak stress of the CPB on the stress-strain curve. As a major means of ground support, CPB must meet mechanical stability requirements to ensure safe underground working conditions. A major evaluation indicator of mechanical stability is the magnitude of UCS, i.e., increased UCS indicates the improved stability of the CPB mass. Therefore, the UCS design is an integral component in the design stage of mine backfilling operation. The reason for such an examination of the UCS is to show how the sulfate attack will affect the maximum stress-carrying capability of the CPB at early and advanced ages. An increase in sulfate content can improve the strength of the CPB in the early stages of development (Dong et al., 2019). To maintain the stability of host rocks, the typically required strength of CPB is 0.7-2.0MPa (Ercikdi, Kesimal, et al., 2009). However, pinpointing the time specifically that the improvement occurs in early development is vital in mining operations as it will allow for greater accuracy in predicting the continuation of mining operations and thus increase mine profitability. Figure 2.9 (Li & Fall, 2018) shows the early-age development of the UCS of CPB at various sulfate contents. As can be seen in the figure, up to 3-days, there is no discernable advantage of the addition of sulfate to the CPB. However, by 7-days, the sample with a moderate amount of sulfate achieves the highest UCS compared to the other samples. Beyond the 3-day mark, the UCS is improved by the addition of sulfate and maintains the highest comparative UCS until 28-days (the start of advanced age development).

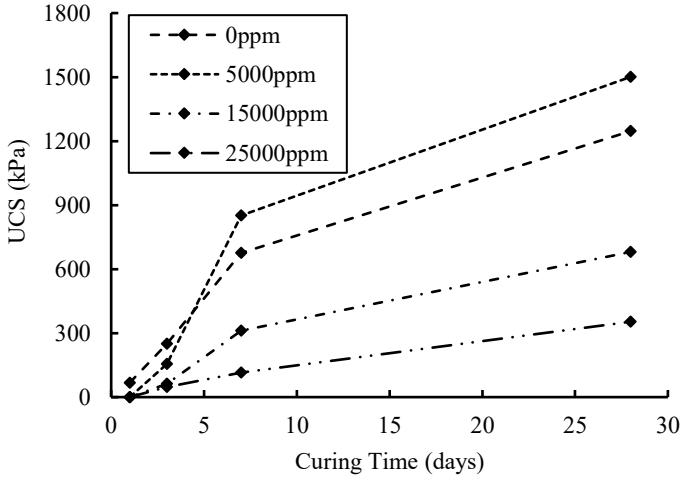

Figure 2.9. Effect of sulfate content on the UCS of CPB at 1, 3, 7, and 28 days (Li and Fall, 2018).

The measure of UCS can also be determined by measuring the suction development within the pore structure of the CPB. An increase in suction development due to self-desiccation can result in an increase in strength in the CPB (Ghirian & Fall, 2016). An increase in self-desiccation within the CPB is due to binder hydration and the formation of CSH. The increase in suction indicates a reduction in the pore water within the CPB internal matrix. As the hydration reactions consume pore water, the suction increases, and the void ratio is decreased as the pores are filled with hydration products. Current literature suggests that a moderate increase in sulfate content has a positive effect on suction within the CPB. However, too high of a sulfate concentration and there is a negative effect on suction development (Li & Fall, 2016, 2018). The mechanism behind such behavior is due to binder hydration inhibition. For example, in Li and Fall (2018), the 5000ppm sulfate concentration sample inhibited binder reaction initially (4.8 days); however, after 4.8 days, binder hydration and expansive phase development congruently formed within the CPB resulting in an increase in suction. Conversely, in the 25000ppm sulfate sample, binder inhibition was too high at this sulfate concentration. As less pore water was consumed due to the inhibited binder hydration, the resultant suction development was less. As CPB transitions from early to advanced ages, the expansive phases will continue to develop in CPB with high initial sulfate content. The continued growth of the expansive phases, in turn, damages the internal pore structure of the CPB. The microstructural damage directly impacts the value of the UCS obtained at advanced ages of the CPB (Li et al., 2018). Therefore, in advanced age CPB, sulfate content has a negative effect and lowers the UCS (Fall & Benzaazoua, 2005; Liu et al., 2018).

2.9.2 Elastic Modulus

Beyond the UCS, understanding how the elastic modulus is affected by sulfate attack is required. The elastic modulus is a fundamental mechanical property that is used to indicate material stiffness. In terms of engineering meaning, the CPB with a higher elastic modulus can provide more effective and immediate ground support when subjected to a given load because a large amount of applied stress will cause less deformation of the CPB. Therefore, it is necessary to evaluate the evolution of the elastic modulus of the CPB under sulfate attack. In early-age CPB, determination of the elastic modulus may be difficult due to the absence of elastic behavior of the CPB on the stress-strain curve. Namely, every early-age material may demonstrate an unnoticeable elastic response under the external loading, and a nonlinear mechanical response dominates its stress-strain

behavior. Due to the low strength of early-age CPB (Cui & Fall, 2019), the secant modulus approach may be utilized to determine the elastic modulus of early-age sulfate CPB. The secant modulus (E_{50}) is defined as the slope of the tangent to the 50% UCS and the origin of the stress-strain curve. Using stress-strain behavior of early age CPB under sulfate attack, the E_{50} may be estimated. Figure 2.10 (Wang et al., 2020) shows the calculated E_{50} using such a method.

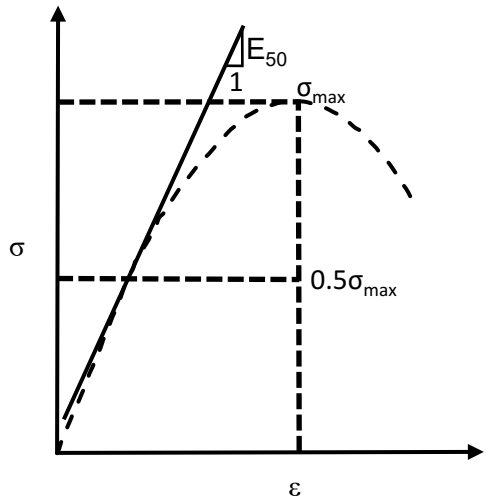

Figure 2.10. Determination of secant elastic modulus (E50) (Wang et al., 2020).

Direct studies (Ghirian & Fall, 2016; Wang et al., 2020) have been conducted on the elastic modulus of CPB under sulfate attack in advanced ages. Figure 2.11 (Fall et al., 2007) shows the effect of sulfate on the elastic modulus of CPB in advanced ages measured at 28-days. As sulfate is increased, there is a slight increase in elastic modulus from 1000ppm to 8000ppm sulfate concentration. As the sulfate is increased beyond 12000ppm, the elastic modulus begins to decrease. The reduction in elastic modulus is attributed to the degradation of the cement matrix of the CPB due to sulfate attack. Similar findings were found in Dong et al. (2016). Four sulfide CPB samples of 2%wt, 5%wt, 10%wt, and 15%wt were tested, and the elastic modulus was measured over a period of 28-360 days. The sulfide content induces sulfate attack in the CPB samples (refer to Eq. 2.1 in which pyrite oxidizes to form sulfate). The findings suggest that although moderate amounts of sulfate are beneficial to the elastic modulus into the advanced age of the CPB, beyond 120 days, there is no long-term improvement to the ability to resist non-permanent deformation.

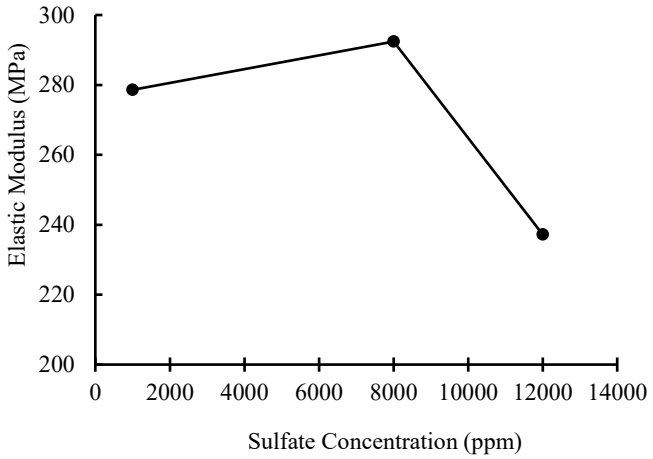

Figure 2.11. Change in Elastic Modulus and UCS at various sulfate concentrations aged 28 days (Fall et al., 2007).

The elastic modulus of CPB under sulfate attack follows a similar pattern to the UCS. Namely, when sulfate is increased moderately, the elastic modulus will increase at an early age. As mentioned in previous sections, a moderate amount of sulfate ion will induce expansive phase development, reducing the void ratio while only minimally inhibiting the binder reaction. When combined, these effects result in a mass that is more resistant to changes in deformation resulting in an increased elastic modulus. However, when sulfate content is increased too high, the elastic modulus will not improve in early-age CPB due to a high level of inhibited binder reaction. Regardless of initial sulfate content, the deleterious effect of the increased gypsum and ettringite production (internal stress, microcracking) becomes clear as CPB transitions from early to advanced ages of development. Thus, the CPB has less ability to resist deformation, and the elastic modulus is decreased.

2.9.3 Shear Strength Parameters

The shear failure envelope of cementitious materials, such as CPB, can be described by the Mohr-Coulomb (M-C) failure criterion. The M-C relationship is described by the following equation:

$$\tau = \sigma \tan \varphi + c \tag{2.4}$$

where τ is the shear stress of the CPB, σ is the normal stress acting on the CPB, and the shear parameters φ and c are the angle of internal friction and cohesion, respectively. The shear strength parameters are used to determine shear strength. When the crack surfaces are generated, cohesion will vanish completely along the crack surfaces, and the mobilization of shear friction resistance

will continuously contribute to post-cracking behavior. Therefore, it is meaningful to discuss the changes in cohesion and angle of internal friction of the CPB under sulfate attack.

Evidence of how the shear strength parameters are affected by sulfate content and time can be seen in studies (Fang et al., 2020; Fang & Fall, 2019; Xu et al., 2020) conducted to measure the shear strength between CPB and rock interfaces. From Xu et al. (2020), it was clear that increased sulfate concentration reduced both cohesion and internal friction values at the early stages (3-days). However, by the 28-day mark, both cohesion and internal friction angle were highest for the sample with 25000ppm sulfate concentration. Figure 2.12 (Xu et al., 2020) shows the evolution of cohesion and internal friction angle of CPB. Therefore, from the study, the pre-7-day shear resistance is significantly reduced with increased sulfate concentration. The authors of this study attribute the low cohesion and low internal friction angle at 7 days for the 25000mg/L specimen to the inhibitory effects of sulfate on binder hydration within the CPB. If binder hydration is retarded, less CSH gel can form, resulting in less shear strength within the CPB up to the 7-day mark. However, when time is increased beyond 7-days to 28-days, the cohesion and shear friction resistance of the CPB begins to increase and is improved with increased sulfate concentration. The authors attribute this to the ability of expansive phase gypsum and ettringite to refine the pore structure and increase the binder contact area against the shear surface. Once the binder contact area is increased due to excess expansive phase development, the cohesion and internal friction angle of the CPB improved in the high sulfate CPB samples by the 28-day mark. Similar findings in terms of cohesion are found in work conducted by Fang & Fall (2019). At an early age, CPB maximum cohesion is achieved in the sample with 5000ppm sulfate concentration compared to 0ppm and 25000ppm after 7 days of curing. However, friction angle results are much different compared to Xu et al. (2020). There is a small change in friction angle, approximately 2 degrees for each sample, and sulfate content had minimal impact on the friction angle of CPB at early ages.

In Figure 2.12 (Xu et al., 2020), there is an apparent large change in friction angle during the early age development of CPB. The authors attribute this large change to an increase in surface area as a result of increased expansive phase development during this time. In Fang and Fall (2019), the increase in friction angle is attributed to longer curing time and continued binder hydration. However, when examining the shear strength parameters, cohesion is attributed to increased binder hydration, and bonding force between particles and friction angle is attributed to the coefficient of

friction between particle and rock surface. Cohesion in CPB may show large increases during development due to increased binder hydration; however, friction angle, regardless of age, should remain relatively the same. Therefore, in CPB, the internal angle changes should be small regardless of the age of development or sulfate content of the CPB. However, this is not what Xu et al. (2020) presented. Although the authors attribute the difference in friction angle to the increased surface area as a result of expansive phase development, there is another explanation as to why the friction angle has increased so drastically during early ages. At the CPB-rock interface, there is more pore water present in 1-day samples when compared to 28-day samples. This increased water results in a lubricating effect at the CPB-rock interface. As the CPB ages, the pore water content is decreased, and the lubricating effect diminishes, thereby increasing the friction angle.

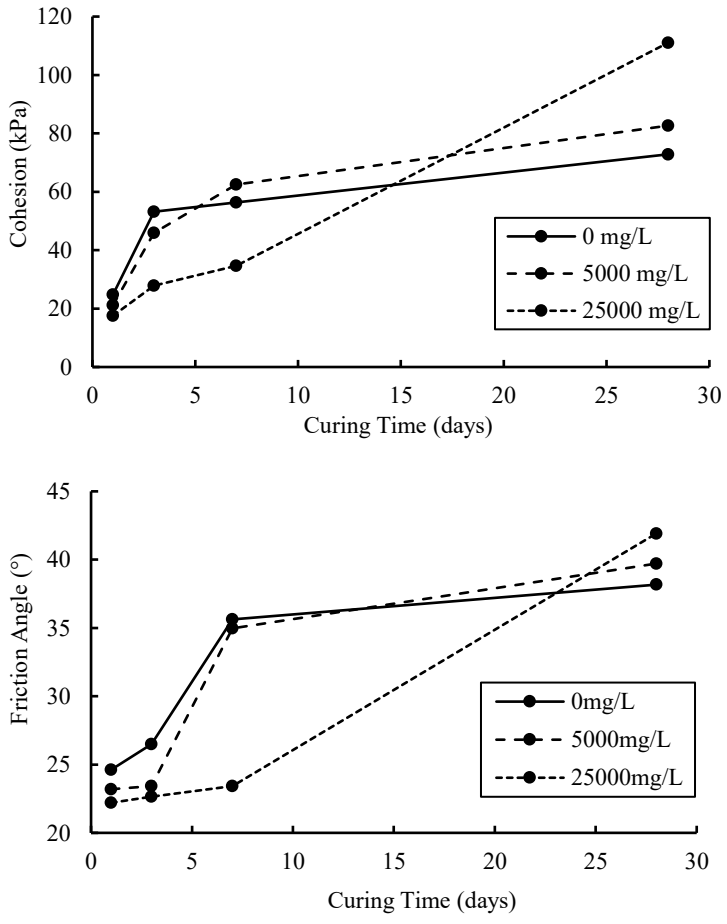

Figure 2.12. Cohesion and internal friction angle at various curing times of CPB at 0, 5000, and 25000 mg/L sulfate concentration (Xu et al., 2020).

2.10 Technical Discussion

Expansive phase production occurs within the CPB. SEM images show the generation of ettringite within the pores of the CPB. One consistent observation is that as sulfate concentration is increased, expansive phases also increase. More specifically, if additional sulfate ions are present within the CPB mixture, there will be an increased production of gypsum and ettringite. Gypsum is formed due to sulfate reacting with CH, which is formed by the hydration of alite and belite. The gypsum in turn, reacts with C_3A to form ettringite. Therefore, to reduce the impact at the microscale on the CPB from the sulfate attack, measures may be taken to inhibit reactions within the CPB that produce expansive phases. Reduction of C_3A to prevent reaction with gypsum is an approach that may be used to reduce ettringite formation. Correspondingly, type HS cement binder (sulfate resistant Portland cement) may be used in high sulfate situations. This is because type HS cements commonly possess a C_3A content below 3% or blast furnace slag content greater than 70% (Penttala, 2009). Using this type of binder over ordinary Portland cement will reduce the production of ettringite within the CPB. By increasing binder additive in the CPB mixture, available cementitious binder components (C_3A, C_3S, C_2S, C_4AF) are reduced. From Aldhafeeri & Fall (2017) the XRD analysis of PC-CPB (Portland cement CPB), PF-CPB (FA-CPB), and PS-CPB (Slag-CPB) showed that there is a reduction of ettringite formation using the PF or PS type cement after 150-day aging. Additionally, the binder portion of the cement paste is not available from direct mining operations and therefore must be obtained outside of the mine. Therefore, the binder tends to be the most expensive component of cement paste (Orejarena & Fall, 2010). By using slag, silica fume, or FA and reducing the Portland cement content in the CPB, further cost savings may be achieved. However, while ettringite formation may be reduced by using slag, silica fume, or FA in the binder mixture current literature suggests that FA does not provide adequate long-term strength (Benzaazoua et al., 2004). Although cost savings may be achieved by using FA in the CPB mixture, the potential safety concerns raised by a further reduction in strength beyond the damage caused by sulfate attack may deter its usage.

The addition of additives may also reduce the formation of gypsum by reacting with CH content in the CPB. Waste industrial products such as silica fume (SF), fly-ash (FA), and slag all contain various levels of S, A and F. Current studies have shown how, through pozzolanic reactions, the active materials in FA (Cui et al., 2020) and slag (Li & Fall, 2018) react with CH to form secondary

CSH. In a comparative study between silica fume (SF), FA, and slag found that SF, FA, and slag all improved the long-term performance of CPB when compared with PC. This is due to the consumption of CH to produce CSH phases within the CPB. The additional consumption of CH and secondary formation of CSH gel results in higher densification and lower porosity on the hardened CPB microstructure (Ercikdi, Cihangir, et al., 2009).

Finally, the last available solution to reduce ettringite and gypsum formation in CPB under sulfate attack is through desulfurization. By chemically treating and removing a portion of the sulfide content in the sulfide-rich mine tailings prior to mixing, there is less available sulfate ion to react with the cementitious materials causing the formation of expansive phases. Floatation processing uses air bubbles to separate hydrophobic and hydrophilic particles into froth and pulp phases in the mining industry (Bhondayi et al., 2015). Through desulfurization via floatation Sahinoglu (2018) found that a high percentage of pyritic coal (81.45%) separation could be achieved for the high pyritic sulfur fine coal. However, to maximize the extent of desulfurization, many factors (feed rate, particle size, quality of pyritic sulfur coal) are required to be considered. This study only focused on pyritic coal formed from mining operations. Therefore, the results can only be claimed for this type of mine tailings. Other forms of mine waste tailings with different properties will require additional testing, and a similar extent of desulfurization may be difficult or not feasible to achieve.

Future work investigating the effect of internal sulfate attack on geomechanical behavior of CPB has been identified as a result of this comprehensive literature review. The current literature links the microstructure development to the mechanical behavior of the CPB. SB-DM has been widely adopted as the current practice with regard to CPB backfill operations. However, this design method assumes a fully uniform CPB mass without internal and surface defects, which degrade the mechanical properties of the CPB. Once placed into stopes, the CPB is subjected to an internal sulfate attack. By utilizing a fracture mechanics-based design method, there may be options to overcome the current limitations of SB-DM. However, no current literature exists as to how sulfate affects the fracture behavior of CPB. Therefore, further research is required in this area.

Chapter 3 Experimental testing program

3.1 Materials

3.1.1 Tailings

Ground silica tailings are used for the preparation of FR-CPB samples. This is because the chemically inert nature of silica tailings can eliminate the uncertainties when the sulfate anions are introduced into the FR-CPB materials and thus facilitate the identification of the effect of sulfate solution. Moreover, the silica tailings consist predominantly of silicon dioxide (99.8%), which is a primary mineral found in Canadian hard rock mine tailings (Li & Fall, 2016) and thus can be used as a representative tailing material for the CPB preparation. A particle size analyzer (model: EPA5002 mastersizer 2000) is used to measure the particle size distribution curve (see Figure 3.1).

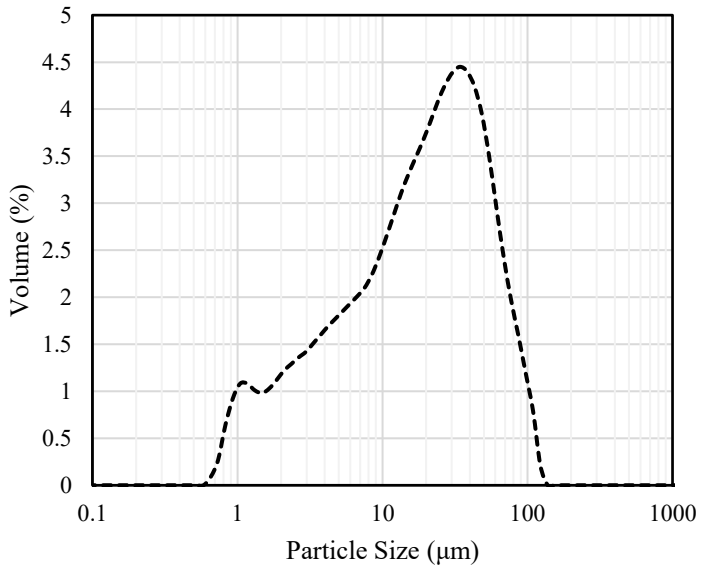

Figure 3.1. Particle size distribution of silica tailings used throughout the study.

3.1.2 Binder

Portland cement type GUL was used for all samples of CPB and FR-CPB. This product is widely available and used as a binder in many commercial mining operations.

3.1.3 Water

For all samples, tap water was utilized as the mix water for the CPB and FR-CPB.

3.1.4 Sulfate

To investigate the effect of sulfate concentration on the fracture behavior of FR-CPB, the ferrous sulfate heptahydrate ($FeSO_4 \cdot 7H_2O$, Manufacturer: Anachemia) is utilized to prepare the sulfate solution. This is partly because of the high-water solubility (approximately 256 g/L) of FeSO4·7H2O in water, which can ensure the uniform distribution of sulfate anions in pore solution. Moreover, this type of sulfate salt contains the divalent cation Fe^{2+}, which is similar to the chemical composition of oxidation products associated with sulfide-rich tailings. Therefore, the adoption of $FeSO_4 \cdot 7H_2O$ can mimic the in-situ chemical reactions in CPB materials.

Figure 3.2. Sulfate salt utilized to create the required concentrations of sulfate mixing water.

3.1.5 Polypropylene fiber

Polypropylene microfibers 12.0mm in length were added to the CPB to create the FR-CPB. The fiber content was controlled to 0.5% of the total CPB mass for all samples cast.

Figure 3.3. Polypropylene microfiber utilized in the FR-CPB preparation.

3.2 Mix recipe and curing method

To observe the effect sulfate has on the mechanical behavior and material properties of the CPB and FR-CPB, four sulfate concentrations (0, 5000, 15000, and 25000ppm) and four curing times (3, 7, 28, and 90 days) were chosen. The mix preparation and curing time were carefully monitored and controlled throughout the duration of the study in order to ensure accurate results. First, the sulfate and mix water was combined to create the desired sulfate concentration within the mix water. The sulfate salt was mixed until completely dissolved in the water. The dry material (silica tailings and Portland cement) were combined separately and hand mixed for 1.0 minute. The dry mix was then added to mix water and hand mixed for approximately 1.0 minute. The mixture was then added to a stand mixer (Kitchen Aid Professional Series) and mixed for 6 minutes. An additional step of mixing in the polypropylene fibers occurred at this stage for the FR-CPB creation in which the fibers would be pulled apart by hand and added to the running mixer until all the required fibers were mixed into the CPB. After 6.0 minutes the bowl was removed and hand mixing to ensure all material on the bowl was incorporated into the mixture commenced for approximately 1.0 minute until the bowl was placed back in the stand mixer for an additional 1.0 minute. This method of mixing ensured that all components of the CPB and FR-CPB were completely mixed together prior to placement.

Placement of the CPB and FR-CPB occurred by pouring the mixture from the bowl into 10.0cm by 20.0cm cylindrical plastic molds in three lifts. Each lift was approximately 1/3 the height of the mold, with each lift receiving 20 roddings with a laboratory bar. Once completely full, the cylindrical mold was tamped 30 times using a mallet. This was done to remove excess entrapped air within the mixture of the CPB. A plastic lid was then placed onto the top of the cylindrical mold and sealed with electrical tape; therefore, no evaporation or pressure release may occur during the curing time of the CPB and FR-CPB. Table 3.1 is a summary of the mix recipe and curing times adopted by this study to examine the effect of sulfate internal sulfate on CPB and FR-CPB.

Table 3.1. Mix design and curing time adopted for the experimental fracture behavior testing.

Group	Mix Recipe	Fiber	Curing Time (days)	Sulfate Concentration	Test and Samples
1A	W/C = 7.6, Cm = 4.5%	Fc=0.5% Fiber Length =12mm	3,7,28, 90	0ppm	SCB = 2*4 = 8 large moulds ENDB = 2*4 = 8 large moulds
1B	W/C = 7.6, Cm = 4.5%	Fc=0.5% Fiber Length =12mm	3,7,28, 90		SCB = 2*4 = 8 large moulds ENDB = 2*4 = 8 large moulds
2A	W/C = 7.6, Cm = 4.5%	Fc=0.5% Fiber Length =12mm	3,7,28, 90	5000ppm	SCB = 2*4 = 8 large moulds ENDB = 2*4 = 8 large moulds
2B	W/C = 7.6, Cm = 4.5%	Fc=0.5% Fiber Length =12mm	3,7,28, 90		SCB = 2*4 = 8 large moulds ENDB = 2*4 = 8 large moulds
3A	W/C = 7.6, Cm = 4.5%	Fc=0.5% Fiber Length =12mm	3,7,28, 90	15000ppm	SCB = 2*4 = 8 large moulds ENDB = 2*4 = 8 large moulds
3B	W/C = 7.6, Cm = 4.5%	Fc=0.5% Fiber Length =12mm	3,7,28, 90		SCB = 2*4 = 8 large moulds ENDB = 2*4 = 8 large moulds
4A	W/C = 7.6, Cm = 4.5%	Fc=0.5% Fiber Length =12mm	3,7,28, 90	25000ppm	SCB = 2*4 = 8 large moulds ENDB = 2*4 = 8 large moulds
4B	W/C = 7.6, Cm = 4.5%	Fc=0.5% Fiber Length =12mm	3,7,28, 90		SCB = 2*4 = 8 large moulds ENDB = 2*4 = 8 large moulds

Abbreviations:
W/C – Water to cement ratio
Cm – Cement content
Fc – Fiber content
ppm – Parts per million
SCB – Semicircular bend test
ENDB – End notch disk bend test

3.3 Mechanical testing program

3.3.1 Semicircular bend (SCB) test

Due to the simple test setup and procedures, efficient usage of testing materials, and high repeatability of testing results, semicircular bend (SCB) tests have been extensively used to investigate the fracture behavior of geomaterials. Therefore, SCB tests are adopted to study the sulfate-induced changes in the mode-I and mode-II fracture behaviors of FR-CPB. Once the CPB and FR-CPB had cured for the desired time, the samples were removed from the plastic molds and trimmed to the desired specifications. For the SCB test, disks 5.0cm in width were cut from the cylindrical mold, which were then cut in half again to create the semicircular shape. As fracture behavior testing requires a pre-defect to be introduced to the material, a notch was then cut into the CPB/FR-CPB at 0 degrees and 54 degrees for mode-I and mode-II, respectively. Cutting of the samples was done using a Bosch GCM12SD miter saw. The high rate of RPM of the saw blade in conjunction with wood cutting molds to hold samples in position ensured that accurate cutting of the samples was achieved with as slight variation as possible from sample to sample.

Once placed into the loading frame, the samples were subjected to a loading rate of 1.0mm/min. The side rollers of the loading frame rotate freely, ensuring no friction between the sample and the frame. An Artech S-type load cell measure the resulting for of the CPB/FR-CPB during the test simultaneously with a linear variable differential transformer (LVDT) position sensor to measure the displacement of the sample. The force and position data was relayed into StrainSmart software datalogging the information at a rate of 10 readings per second. The data was then placed into excel software for analysis. To eliminate any errors or anomalous results, each test was conducted 3 times per sample. In total, 144 CPB and 144 FR-CPB tests were conducted to determine the effect sulfate has on the two materials. In mode-I, the sample will be pulled in tension as the crack tip is placed at an angle of 0 degrees therefore this is mode-I fracture loading configuration. In mode-II, the sample will shear in-plane with the load as the angle of the crack tip is placed at 54 degrees, therefore this is mode-II loading configuration. Figure 3.4 below shows the mode-I and mode-II loading configurations used for the SCPB testing.

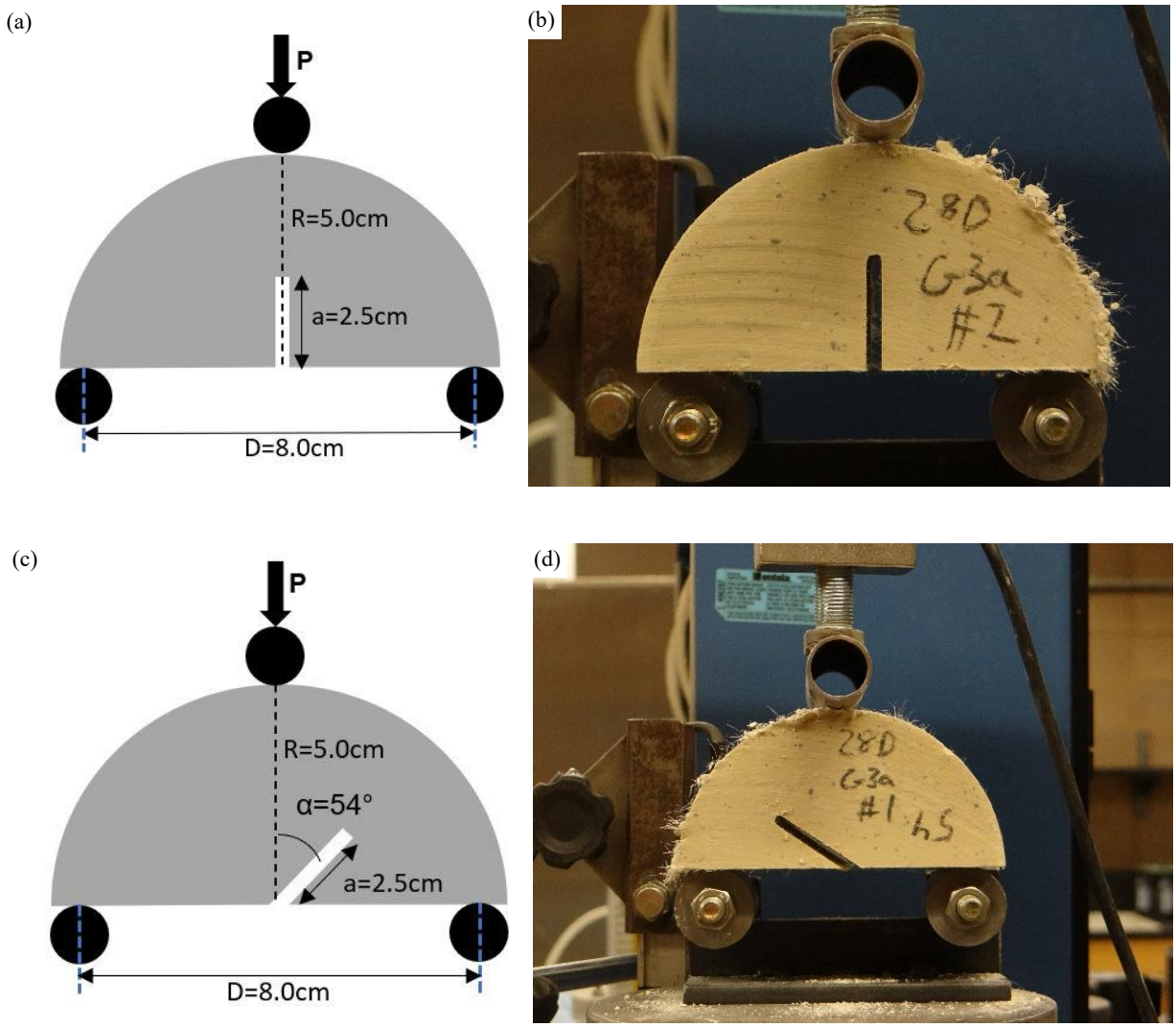

Figure 3.4. Mode-I (a, b) and mode-II (c, d) SCB test dimensions and experimental setup.

3.3.2 End notch disk bend (ENDB) test

A few test configurations such as inclined edge cracked three-point bend beam, circumferentially notched shaft, inclined edge cracked bend beam, edge cracked plate, and end notched disc bend (ENDB) samples are proposed to investigate the mode-III (out-of-plane sliding) fracture behavior. Among these proposed test configurations, ENDB samples can be obtained more straightforwardly from drilling cores of rock materials and artificially prepared cylindrical cementitious materials such as concrete. Moreover, this sample configuration has been successfully applied to the investigation of fracture behavior of fiber-reinforced composites. Therefore, the ENDB test is chosen to study the fracture behavior of FR-CPB materials under mode-III loadings. The test

requires disks 5.0cm in width cut from the cylindrical molds. For ENDB testing, a notch of 2.0cm in depth was required as the defect introduced to the circular disk. The notch was then aligned 60 degrees with respect to the top loading bar. All load frame, sensor and datalogging software remained the same for ENDB testing as was used for the SCB testing in section 3.3.1. All tests were conducted 3 times; therefore, in total, 96 ENDB were conducted for the CPB samples, and 96 ENDB tests were conducted for the FR-CPB samples throughout the length of the study. As the load is placed on the CPB and FR-CPB in the mode-III load configuration, the sample is forced to shear out-of-plane to the load, therefore this is a suitable testing configuration for mode-III fracture behavior. Figure 3.5 below shows the load configuration adopted for the mode-III testing conducted.

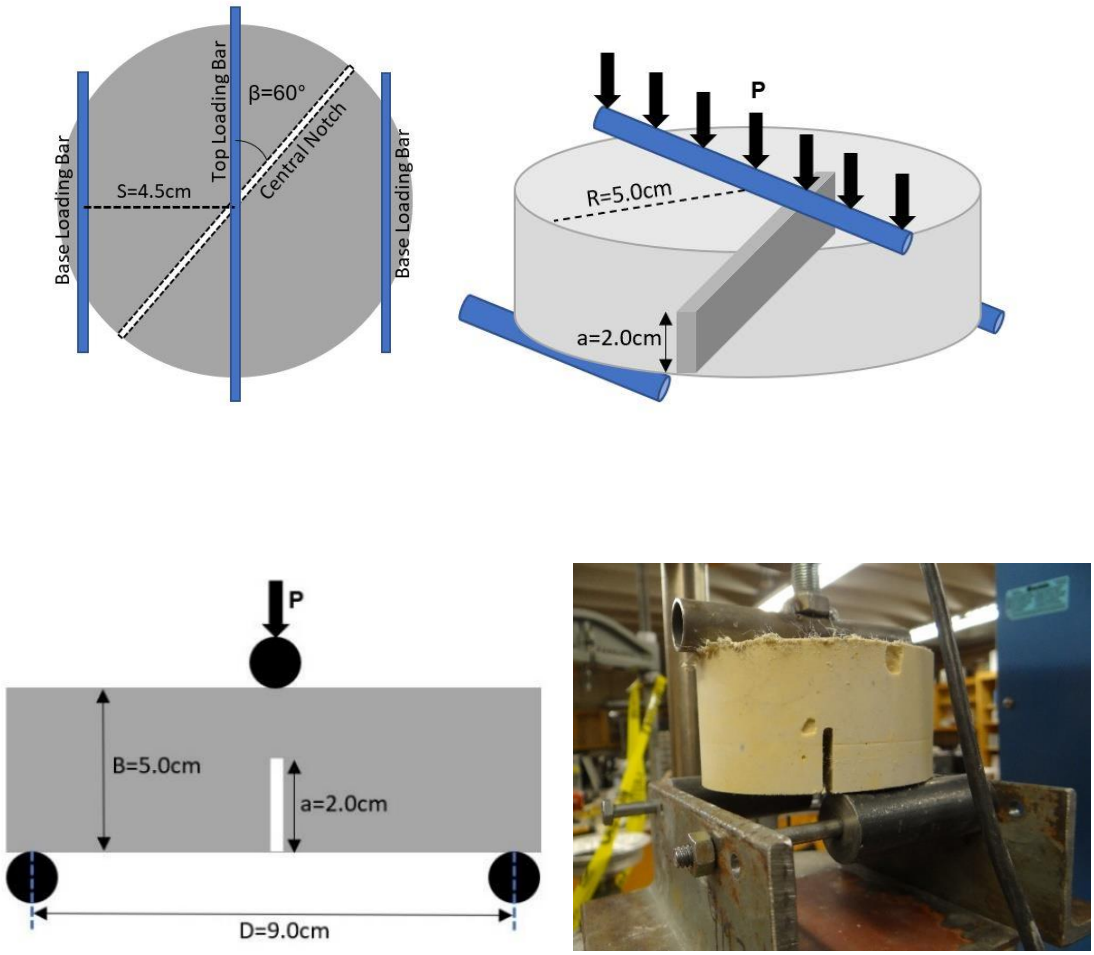

Figure 3.5. Geometry and loading for the CPB/FR-CPB ENDB test.

3.4 Auxiliary analysis

3.4.1 Scanning electron microscope (SEM) analysis

Examining how the expansive phases develop within the pore space of the CPB will provide further insight as to how the microscale development affects the macroscale performance of the CPB. In order to examine the microscopic pores scanning electron microscopy (SEM) was used. Dried samples cut 2.0mm thick of CPB and FR-CPB were prepared and adhered to metal pedestals for placement into the Hitachi SU-70 SEM. All the CPB samples prepared for the SEM were chosen from the same relative position within the CPB cylinder. This is to ensure no excess entrained air is in the pore space of the dried CPB and ensure relatively the same microstructure development of the CPB across the various samples analyzed.

Figure 3.6. Scanning electron microscope used to capture the microscale SEM images of CPB and FR-CPB.

3.5 Determination methods of fracture properties

In addition to determining the fracture behavior of the CPB, the effect of internal sulfate for four material properties was examined. The first material property examined was fracture toughness. Fracture toughness is the ability of a material to resist crack growth in brittle materials. As CPB is a brittle and homogenous material, it is a suitable material to investigate the fracture toughness. When the load is placed on the CPB/FR-CPB once the peak load is released, there is a release in strain energy when the crack propagates through the material from the pre-cut notch. The fracture toughness utilizes the measured peak load and is an indication of the damage resistance the brittle

material possesses. Mode-I and mode-II (K_{IC}, K_{IIC}) fracture toughness values are determined from the following formulas:

$$K_I = \frac{P}{DT}\sqrt{\pi a}Y_I \tag{3.4}$$

$$K_{II} = \frac{P}{DT}\sqrt{\pi a}Y_{II} \tag{3.5}$$

Where P is maximum force applied to sample (N); D is the diameter of the sample between loading bars (m); T is the thickness of the sample (m); a is the notch length (m); Y_I is the normalized stress intensity factor for mode I fracture toughness (Y_I = 6.52); Y_{II} is the normalized stress intensity factor for mode II fracture toughness (Y_{II} = 1.072). For mode-III (K_{III}) the formula to determine the fracture toughness is determined using the following equation:

$$K_{III} = \frac{6PS}{RB^2}\sqrt{\pi a}Y_{III} \tag{3.6}$$

Where P is the maximum force applied to sample (N); T is the thickness of the sample (m); a is the notch length (m); B is the thickness of the disk (m); S is the distance between loading and support bar (m); R is the radius of the specimen (m); Y_{III} is the normalized stress intensity factor for mode III fracture toughness (Y_{III} = 0.0713).

The stiffness of the backfill material is an indication of the immediate ground support the material can provide when subjected to the complex loading conditions present in the underground mining stope. Therefore, stiffness is a vital material property to evaluate and determine the effect internal sulfate has in order to assist in the engineered design of the material. In order to determine the stiffness of the CPB and FR-CPB, the slope of the load-displacement curve was utilized.

When considering the method of backfill design, it is advantageous to understand the amount of deformation the CPB and FR-CPB can withstand prior to fracture. This is especially apparent when considering that in the underground stope, the surrounding rock wall imparts enormous forces into the backfill body mass. There will be some deformation of the material prior to complete failure. As the backfill is a brittle material understanding the tolerances of deformation can be critical to understanding if the backfill pillar remains stable or has been displaced to such a degree that failure is likely. Therefore, energy (or work) to crack initiation (Wc) is a material property that will show

how much deformation the CPB/FR-CPB can withstand and the effect the internal sulfate has on this material property. To determine the Wc, the area under the load-displacement curve from onset of loading to peak load is calculated.

Lastly, for FR-CPB, there is a transition zone on the load-displacement curve in which, after the peak load is achieved and the strain energy released, the load is transferred from being resisted by the internal matrix of the CPB to the fibers added to the CPB matrix. This transition zone is referred to as the work to fiber bridging (Wf). A larger work to fiber bridging indicates a stronger interfacial bond between the CPB and the polypropylene fibers. CPB without fiber does not experience this bridging effect. The four material properties of fracture toughness, stiffness, the energy of crack initiation, and work to fiber bridging are all determined using the load-displacement curve shown in Figure 3.7.

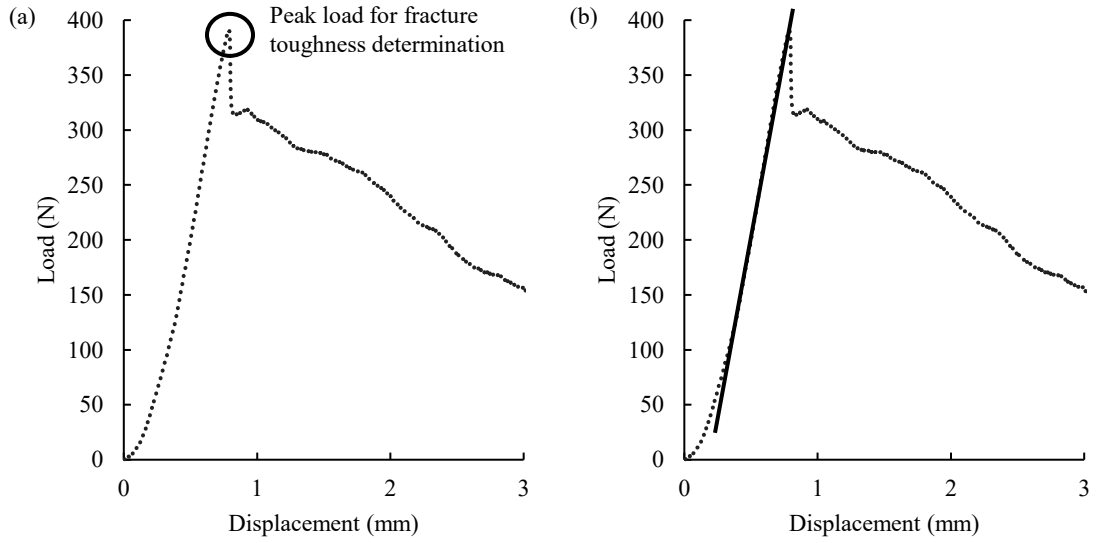

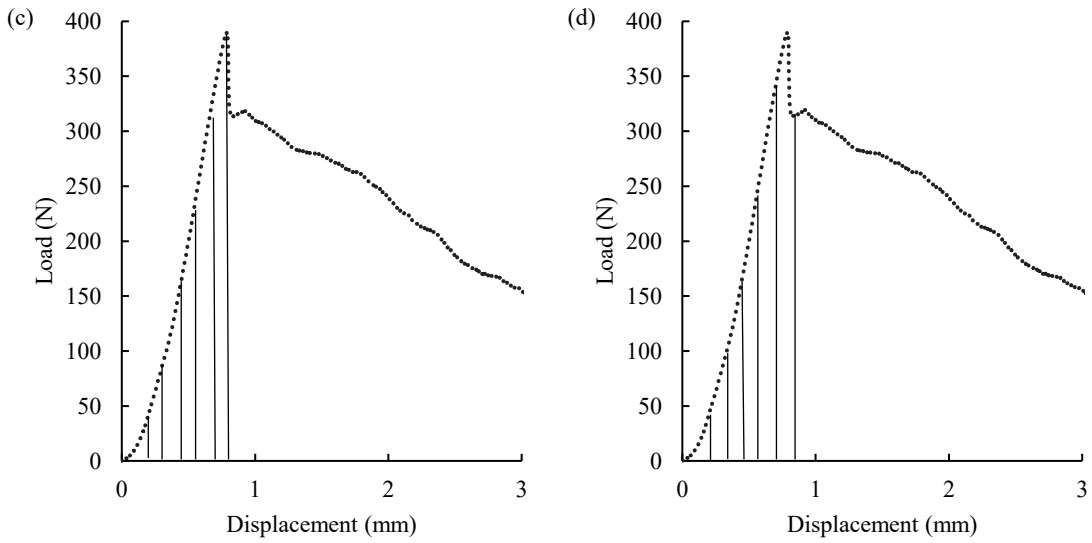

Figure 3.7. Definition of fracture properties; (a) fracture toughness, (b) stiffness, (c) energy of crack initiation, and (d) work of fiber bridging.

Chapter 4 Experimental results

4.1 Effect of sulfate content on fracture behavior and properties of CPB

4.1.1 Effect of sulfate content on mode-I fracture behavior of CPB

The results obtained show that sulfate has an effect on the mode-I fracture behavior of the CPB, and it can be seen that there are changes in the behavior from early to advanced-age CPB due to the inclusion of sulfate. At a very early age CPB, it can be seen that sulfate has a negative effect on the fracture behavior of the CPB. In CPB with high quantities of sulfate (15000 and 25000ppm), at 3 days curing time, the peak load the CPB is able to resist is reduced. Additionally, the slope of the pre-peak load-displacement behavior is lessened significantly as sulfate content is increased from 15000ppm to 25000ppm. CPB with a 0ppm internal sulfate concentration from the strength-bearing hydration products of CSH and portlandite (CH) within the bulk matrix of the CPB. However, with the introduction of excess quantities of the CH is consumed, producing gypsum rapidly within the pore space of the CPB. The reaction rate of the CSH is slower by comparison to the formation of the gypsum and ettringite. Therefore, strength-forming hydration products are consumed congruently with the rapid formation of expansive phases within the mix of the early age CPB. It is hypothesized for these reasons that there is a severe reduction in load-displacement behavior of the CPB at 3 days. Of great importance is the rapid improvement of the CPB with high sulfate concentration from 3 days to 7 days and beyond. This evolutive behavior can be seen in Figure 4.1 below, showing the changes in pre-peak and peak load of the different CPB samples at the different sulfate concentrations and curing times. The reasoning behind such behavior can be inferred from the preparation of the CPB. When prepared, the CPB is placed into plastic molds. The molds are stiff and do not allow for any displacement to occur during the curing of the CPB. This mirrors the placement of the CPB into hard rock stopes, where during the curing of the CPB, there will not be any displacement of the hard rock due to the curing of the CPB. As the samples with high quantities of sulfate cure, excess expansive phase development will occur within the pore space of the CPB. This will produce additional pressure within the CPB mold, of which there is no effective release. The increase in pressure forces the microstructure of the CPB to become denser over the duration of the curing time in a process known as passive confinement. Once the CPB is removed from the plastic molds for testing, the increased pressure the CPB with sulfate is forced to cure under is not immediately released. Instead, the densification of the microstructure

is locked once adequate curing has occurred. As density and porosity contribute to the mechanical behavior of the CPB, the locked densification of the CPB with higher sulfate concentrations results in improved fracture load-displacement behavior of the CPB.

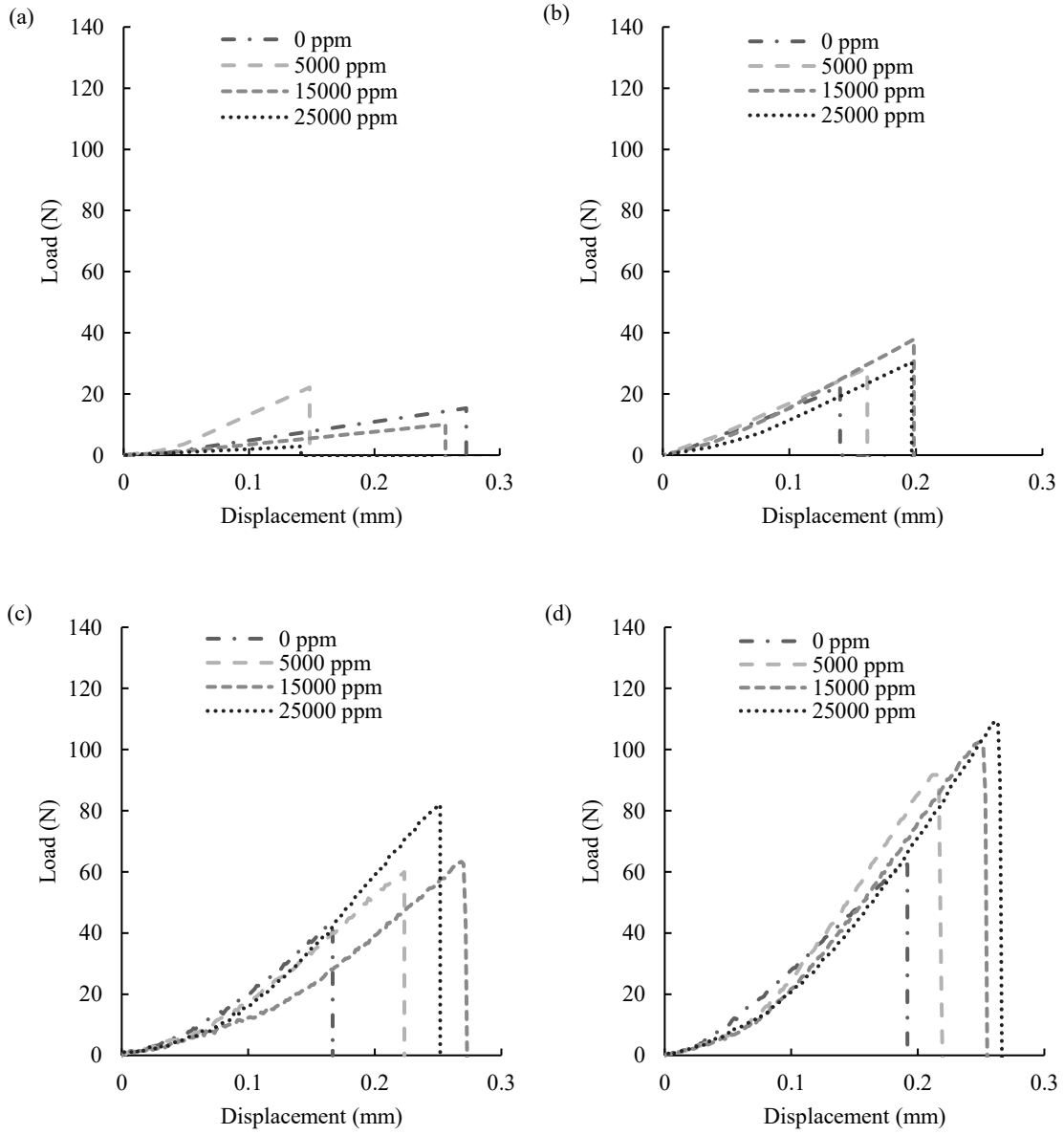

Figure 4.1. Effect of sulfate on the mode-I load-displacement behavior at (a) 3 days, (b) 7 days, (c) 28 days, and (d) 90 days.

4.1.2 Effect of sulfate content on mode-II fracture behavior of CPB

The trend of the load-displacement behavior for mode-II loadings is similar to mode-I. When observing the very early-age CPB, the CPB behavior again shows a lessened pre-peak branch and

lowered peak force with the CPB of 15000 and 25000ppm. Contributing to this behavior is the excess formation of expansive phases and the overconsumption of strength-producing products within the CPB mixture. Again, beyond 7 days, it is observed in the load-displacement behavior that the pre-peak of the CPB curves with sulfate become more vertical in nature. As well, the peak load-displacement becomes higher than the control CPB. The aforementioned factors in section 4.1.1 of increased passive confinement and improved densification of the CPB are applicable to the mode-II load-displacement behavior of the CPB and can be seen in Figure 4.2. When comparing the behavior of the CPB between mode-I, mode-II, and mode-III, there is a noticeable increase in load-displacement behavior as you analyze from mode-I to mode-II and again between mode-II and mode-III. As mode-I is a pure tensile failure of the CPB, cohesion is the dominant factor determining the load-displacement peak of the CPB. However, mode-II (in-plane shear) and mode-III (out-of-plane shear) have hydration bond cohesion as well as interparticle friction contributing to the overall fracture behavior of the CPB. It is, therefore important to note that the inclusion of sulfate does not drastically change the load-displacement behavior of the CPB between the modes of failure, which indicates that the addition of the friction increases the peak load of the CPB in mode-II and mode-III configurations. However, it does not change the position of the peak load relative to the other sulfate concentrations in the load-displacement behavior (i.e. The position of the 15000ppm peak load for 7 days mode-I will correspond to the 15000ppm peak load for 7-day mode-II load displacement relative to 0ppm, 5000ppm, and 25000ppm).

Figure 4.3 shows the SEM analysis conducted on the 25000ppm CPB at 3, 7, 28, and 90 days. From the images, it can be seen that the pore space of the very early-age CPB is large even with the early hydration of the expansive phases. This can be attributed to the rapid consumption of the hydration products required to make the strength-bearing products of CPB in substitution for the formation of the gypsum and ettringite. However, as the age is increased from early to advanced age CPB, it can be seen that the ettringite and gypsum formation does not diminish with advanced ages but rather stays present during the entire development of the CPB. As the curing time continues to increase, the strength-related hydration products continue to form in conjunction with the expansive phases, consuming pore water and increasing the passive confining pressure within the CPB. This locks the matrix of the CPB into a dense configuration that cannot be released once the CPB is released from the plastic curing mold. This increased densification results in improved fracture behavior in the advanced-age CPB with sulfate when compared to the control CPB.

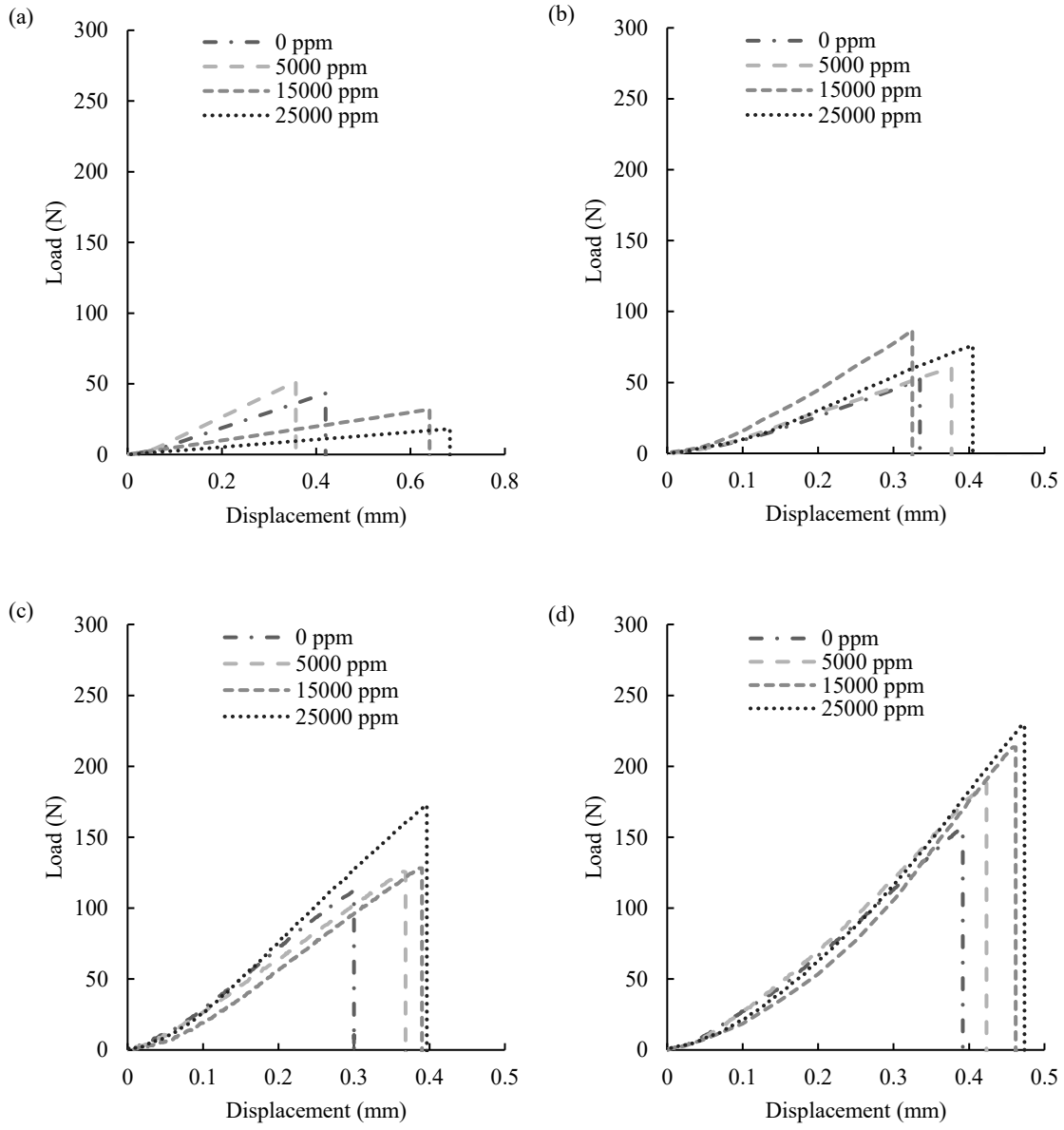

Figure 4.2. Effect of sulfate content on the mode-II load-displacement behavior at (a) 3 days, (b) 7 days, (c) 28 days, and (d) 90 days.

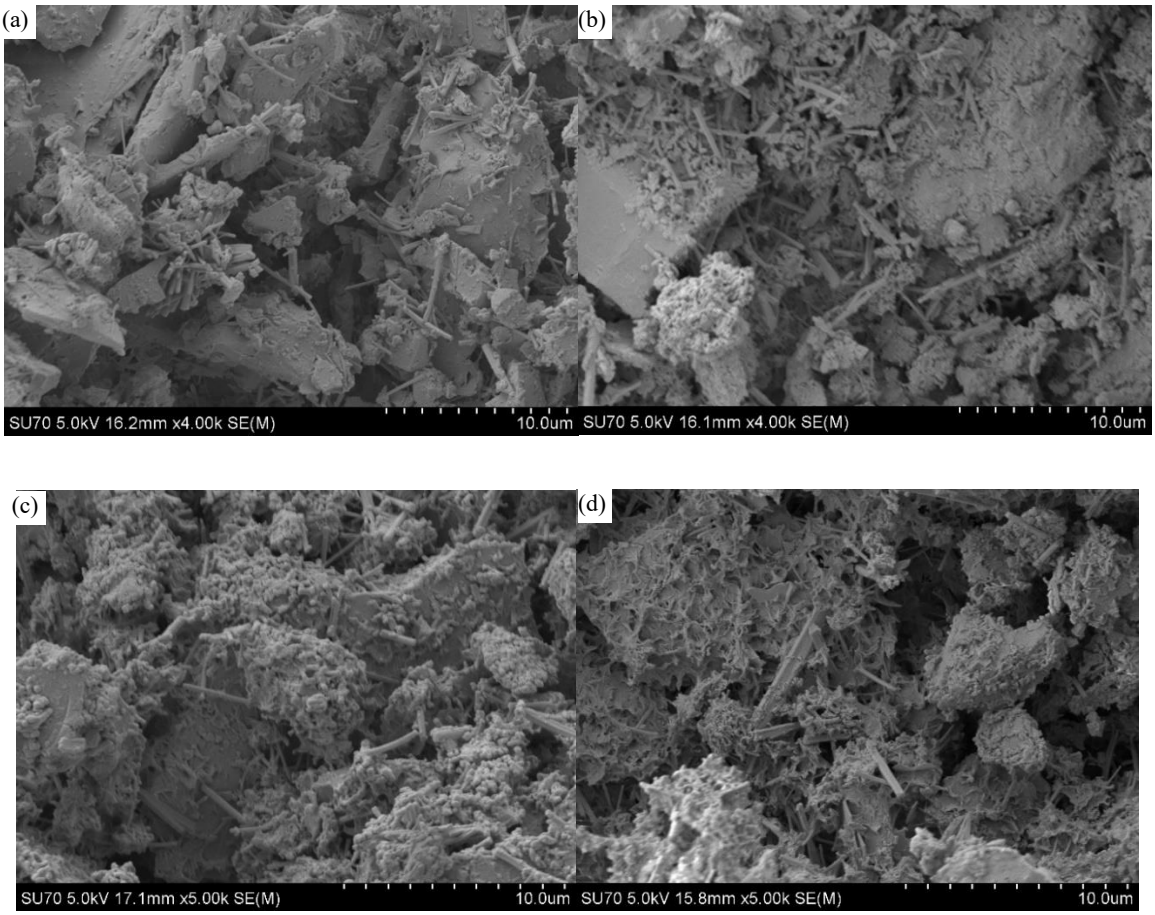

Figure 4.3. SEM analysis of 25000ppm CPB at (a) 3 days, (b) 7 days, (c) 28 days, and (d) 90 days.

4.1.3 Effect of sulfate content on mode-III fracture behavior of CPB

The target ore extracted in any mining operation can vary. However, in rock environments, such as the Canadian shield, the rock boundary walls of the stope can be extremely coarse and jagged. This can in turn coarsen the CPB surface, creating a rough CPB/rock boundary zone in which mode-I, mode-II, and mode-III crack propagation will occur. Additionally, as mentioned in previous sections, the complicated and extremely varied nature of the loading on the CPB body can create internal shear within the CPB bulk matrix (mode-II and mode-III failure modes). Therefore, by examining the mode-III fracture behavior of the CPB, even greater insight into the effect of internal sulfate on CPB can be determined, resulting in improved field implementation of the CPB. Figure 4.4 shows the evolutive behavior of the mode-III behavior of the CPB. In the very early-age CPB at 3 days it can be observed that the very high sulfate concentration significantly reduces the pre-peak and peak load behavior of the CPB. For the 25000ppm sulfate samples, the early consumption of CH and rapid formation of the expansive phases weakens the CPB to such a

degree that at 3 days, there is hardly a registerable load observed in the load-displacement curve. At 7 days, the rapid change for the 15000ppm and 25000ppm samples seen in mode-I and mode-II is again observed in the load-displacement behavior of the CPB. The passive confinement pressure locks the hydration products into a denser CPB matrix. Once removed from the plastic mold, retains the increased densification obtained through the elapsed curing time and additional expansive phase development. Important to observe in the mode-III load-displacement curve is the post-peak residual strength observed after the CPB sample has fractured, not seen in the mode-I or mode-II load-displacement curves. As a catastrophic failure of the CPB is the greatest risk to underground worker safety, any residual strength of the CPB can be extremely useful with regards to monitoring and engineered design in the underground stope. When the CPB sample fractures in the mode-III configuration, a large fracture surface is generated and is still in contact with the CPB. The two halves of the broken CPB are unable to completely clear each other after the initial break and are forced to slide past each other over the created fracture plane. It is the residual friction created from the two halves registering as post-peak load-displacement behavior of the CPB. The behavior can be seen at the 3-day curation time onwards and is a function of the load configuration of the CPB.

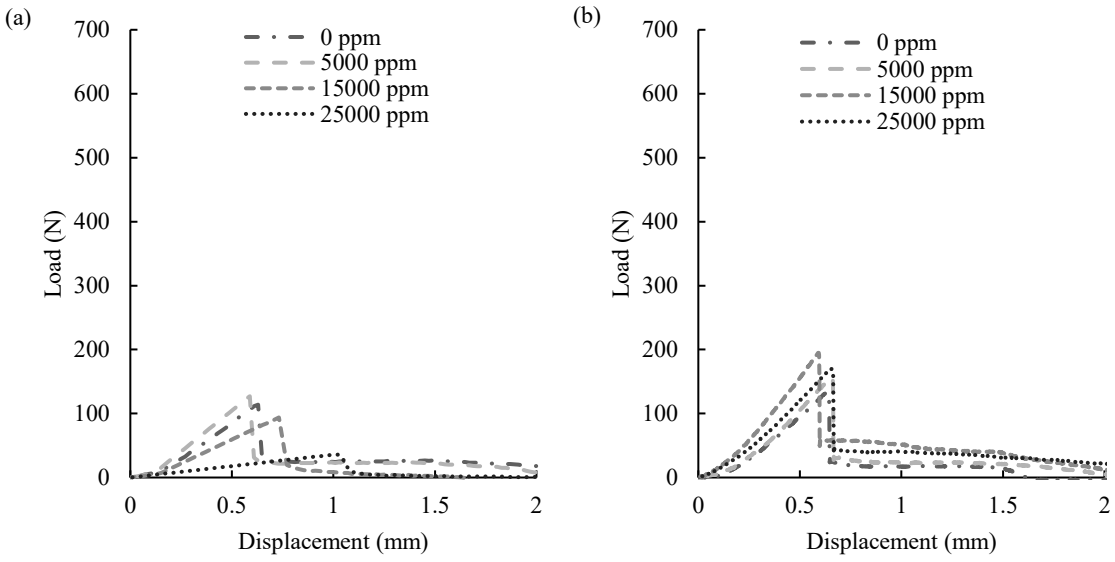

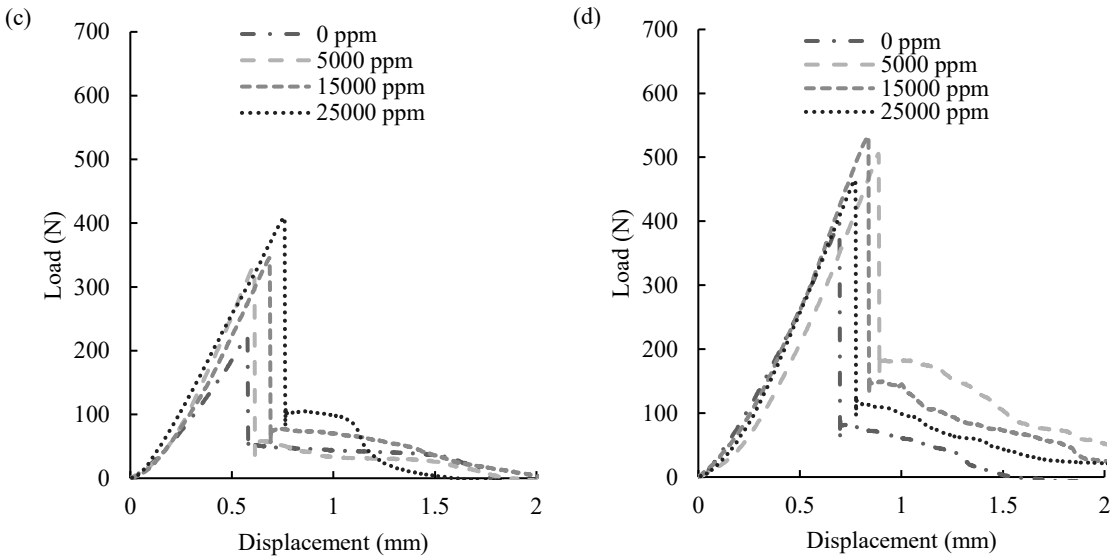

Figure 4.4. Effect of sulfate content on the mode-III load-displacement behavior at (a) 3 days, (b) 7 days, (c) 28 days, and (d) 90 days.

4.1.4 Effect of sulfate content on fracture properties of CPB

4.1.4.1 Effect of sulfate content on the material stiffness of CPB

Figure 4.5 shows the evolutive trend of the stiffness of the CPB. The trend of evolution of the CPB stiffness shares a similar shape when comparing stiffness across the modes of fracture. At a very early age CPB with high sulfate content, it is observed that there is a reduction in material stiffness when compared to the control CPB. However, there is a rapid improvement in material stiffness during the early age development of the CPB (first 28 days) following a reduction in the rate of stiffness change from 28 to 90 days regardless of internal sulfate content. The enhanced passive confining pressure increases the density of the CPB while locking the expansive phases into the bulk matrix of the CPB results in improved material stiffness for the CPB with high amounts of sulfate. At 90 days, the stiffest CPB is 25000ppm followed by 15000ppm, 5000ppm, and 0 ppm for mode-I, mode-II, and mode-III. Mode-II and mode-III stiffness curves show a relatively higher increase in material stiffness when compared to mode-I. This trend is clearest when examining the advanced age extreme sulfate content CPB samples. In the early age of CPB development, the rapid hydration of expansive phases consumes excess pore water. This reduction in pore water also increases the friction of the mode-II and mode-III samples.

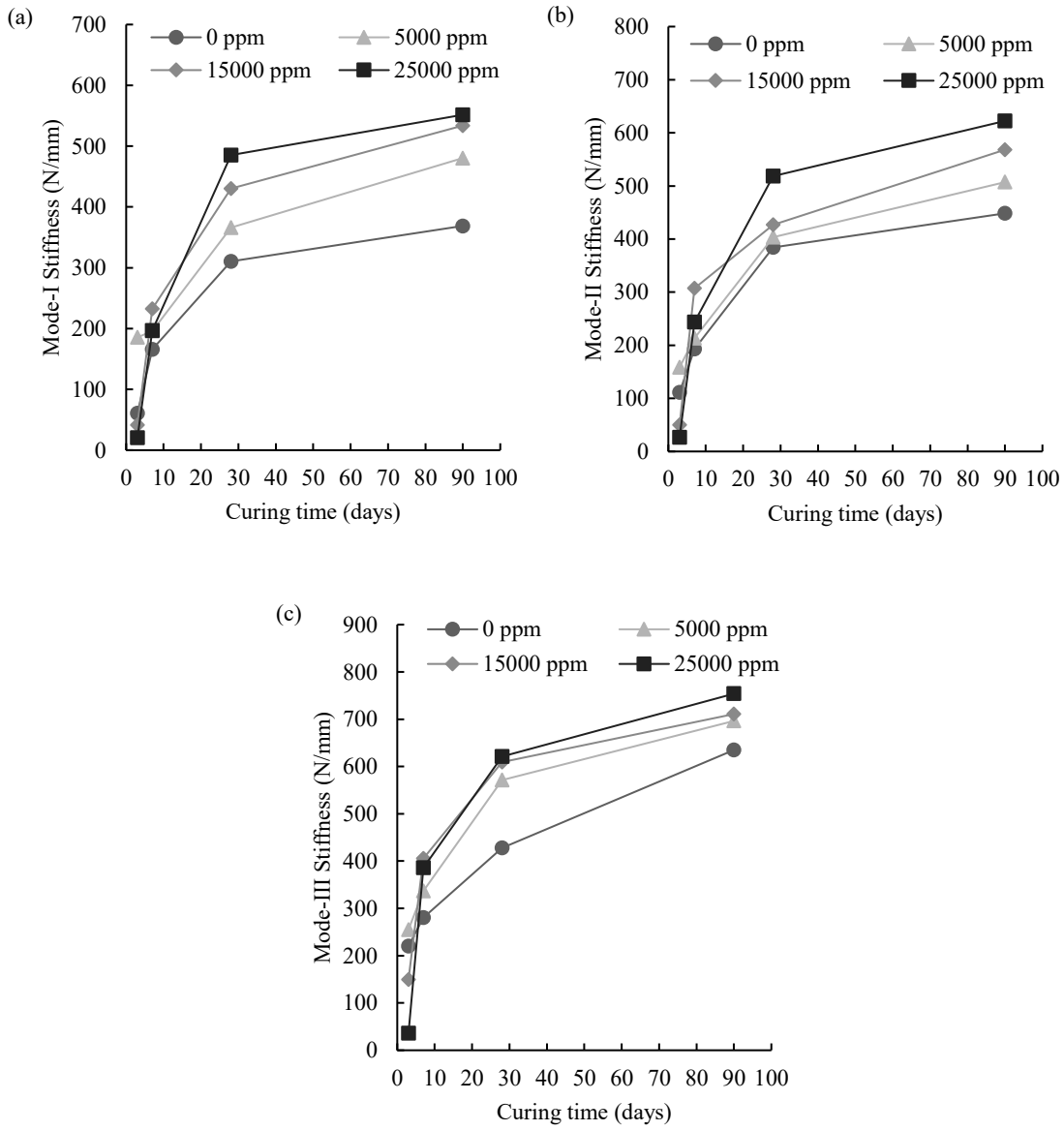

Figure 4.5. Effect of sulfate on the evolutive stiffness of CPB under (a) mode-I, (b) mode-II, and (c) mode-III.

4.1.4.2 Effect of sulfate content on the fracture toughness of CPB

Figure 4.6 shows the fracture toughness of the CPB at the various curing times and sulfate concentrations. The evolution of the fracture toughness for the CPB follows a very similar trend when examined across the modes. Fracture toughness is determined using the peak of the load-displacement curve; therefore, it is a strength-related material property. As it is a strength-related material property, the increase in densification and reduction in gravimetric water content experienced in the very high sulfate CPB will undoubtedly affect the fracture toughness of the CPB, especially in advanced ages. At a very early age CPB, it can be observed that there is a

significant reduction in fracture toughness in the CPB in mode-I, mode-II, and mode-III at the very early age curing time (3 days) however, at 7 days, there is an improvement in the fracture toughness of the CPB with high sulfate content. In this study, the sulfated CPB shows a greater resistance to crack propagation when compared to the control CPB consistently from 7 to 90 days of curing time.

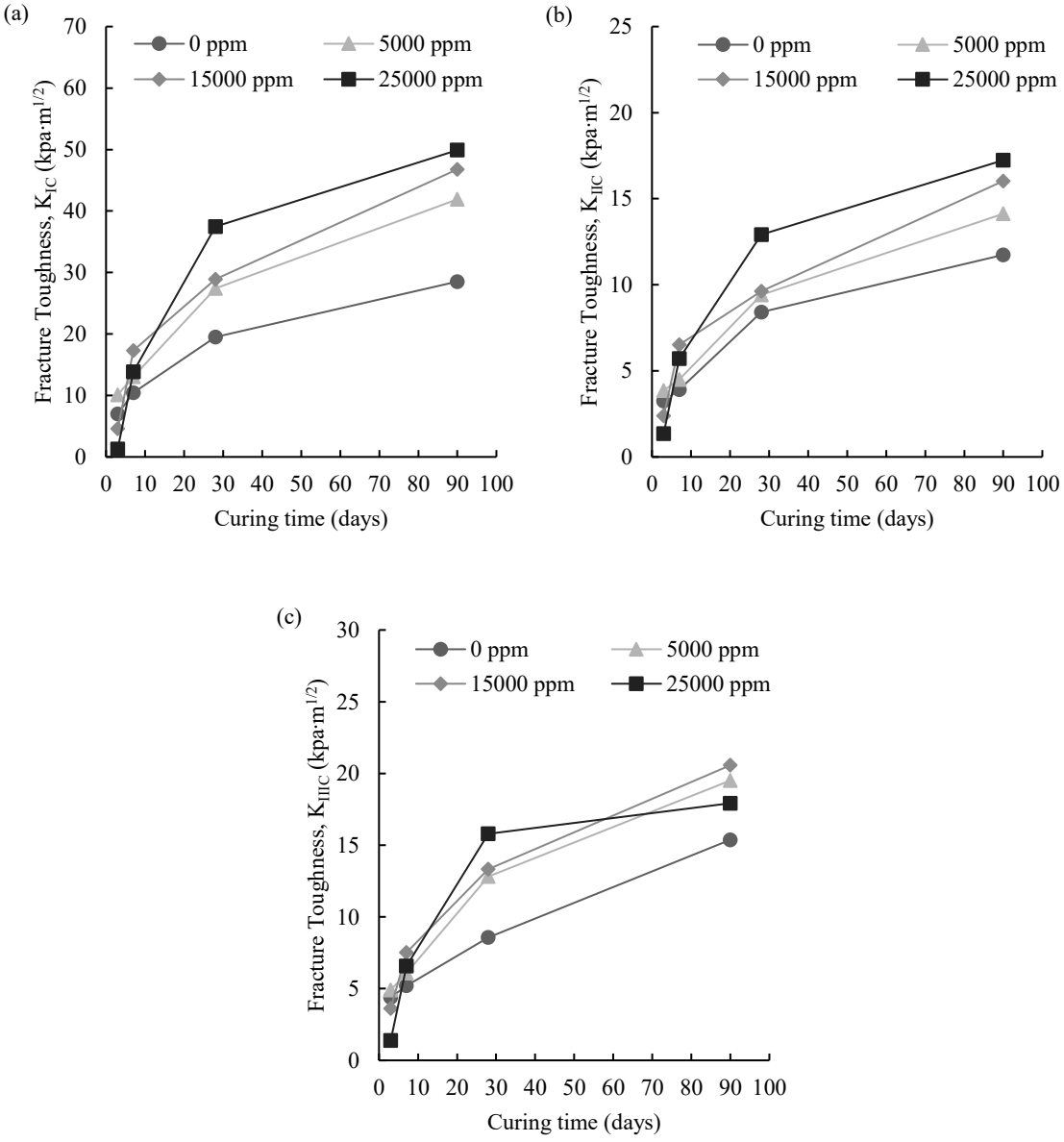

Figure 4.6. Effect of sulfate content on the evolutive fracture toughness of CPB under (a) mode-I, (b) mode-II, and (c) mode-III.

Due to difficulty in the preparation and testing of the shear CPB samples (mode-II and mode-III), it is useful to evaluate if the fracture toughness determined for mode-I (K_{IC}) may be used for the prediction of the mode-II (K_{IIC}) and mode-III (K_{IIIC}) fracture toughness. Therefore, the ratio of K_{IC}/K_{IIC} and K_{IC}/K_{IIIC} was determined in this study. From the study, it was found that the ratio of K_{IIc}/K_{Ic} is 0.34 to 1.04, and K_{IIIc}/K_{Ic} is 0.36 to 1.07, respectively, as shown in Figure 4.7. To prepare shear fracture toughness samples and test the preparation is a much greater difficulty when compared to mode-I. Therefore, it is of great importance to propose a method in which K_{Ic} may be used to predict the tensile and shear failure of the CPB. Previous literature on fracture behavior of materials (Schöllmann et al., 2002; Sih, 1974, Hussain et al., 1974) states that the fracture toughness ratio must be less than or equal to one (satisfied in all cases except very early-age 3 day 25000ppm CPB) and that K_{IIIc}/K_{Ic} must be greater than K_{IIc}/K_{Ic}. From Figure 4.7, there is a weak dependency between the fracture toughness values and the internal sulfate concentration. Therefore, K_{IC} may be used as the predicted value for the shear fracture toughness of the CPB.

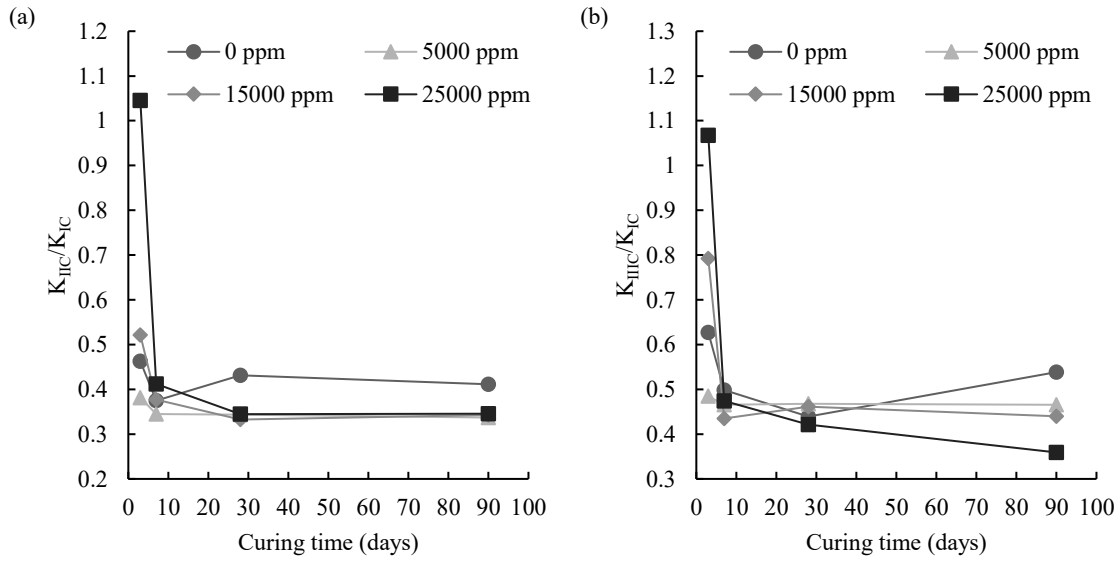

Figure 4.7. Fracture toughness ratios (a) K_{IIC}/K_{IC} and (b) K_{IIIC}/K_{IC}.

4.1.4.3 Effect of sulfate content on the fracture energy of CPB

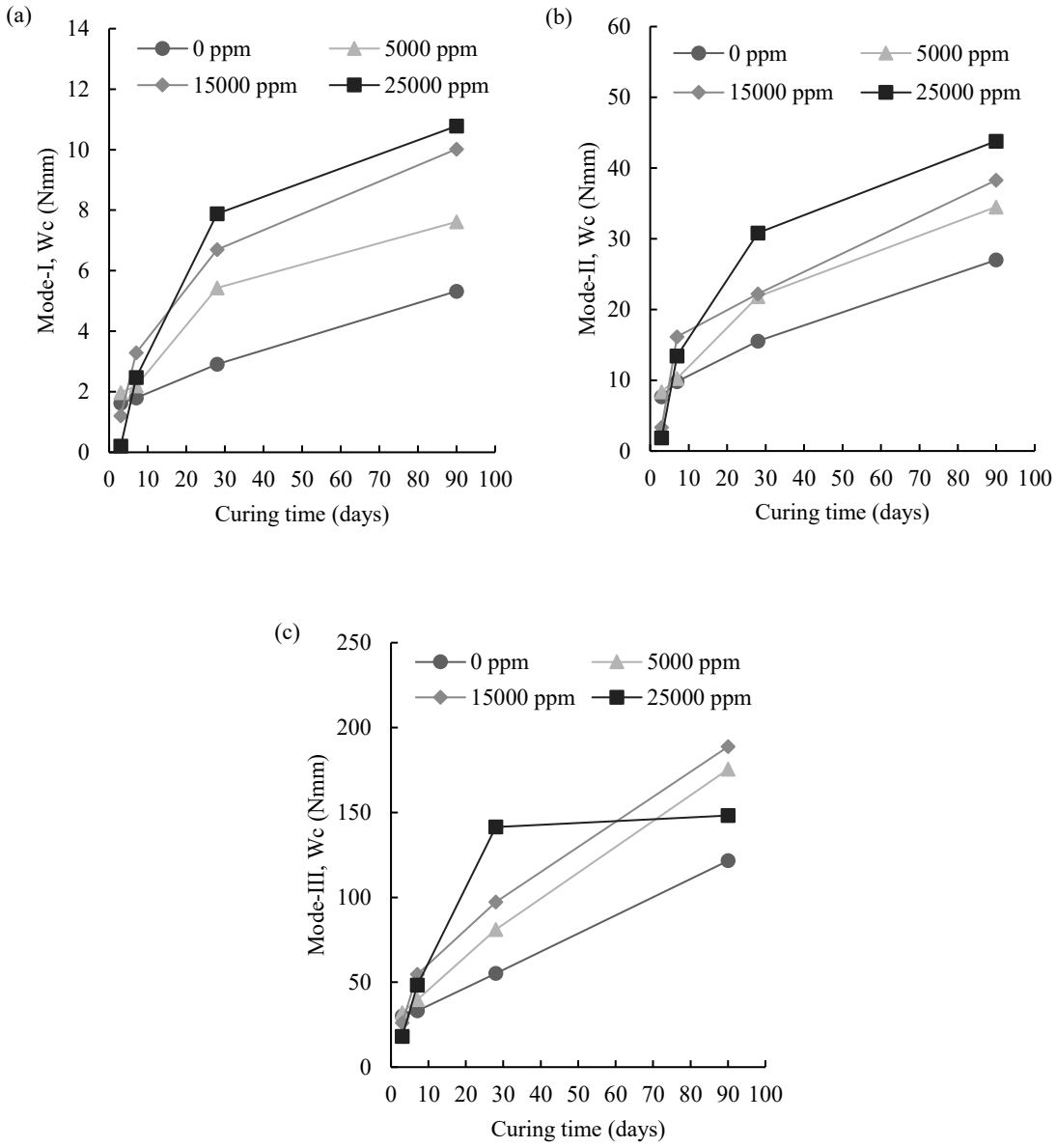

Figure 4.8. Effect of sulfate on energy to crack initiation (Wc) of CPB under (a) mode-I, (b) mode-II, and (c) mode-III.

Figure 4.8 shows the evolutive work to crack initiation (Wc) of the CPB with different sulfate contents. The Wc is a measure of how much total energy is required to drive the crack propagation through the CPB mass. At a very early age, it is clear that sulfate has a negative effect on the Wc of the CPB, with 15000ppm and 25000ppm sulfate samples showing the lowest Wc for mode- I, mode-II, and mode-III. Rapid improvement of the sulfated CPB is shown from 3 days to 7 days. At

28 days, the 25000ppm sulfate CPB requires the most work to initiate cracking in the CPB. At 90 days, the CPB with sulfate requires more energy than the control CPB to crack, releasing the strain energy within the CPB body. Figure 4.8 also shows the increase in fracture energy as you examine the material property from mode-I to mode-II and mode-III. As mode-I tensile fracture relies solely on cohesion to resist the fracture of the CPB, mode-I has the lowest fracture energy when compared to the other modes at the same relative curing time. In mode-II interparticle friction and cohesion resist the fracturing of the CPB. For this reason, increased energy is required to fracture the configuration in the mode-II configuration. Further to this point, in mode-III, there is a very large fracture plane formed when the CPB material is reaching the peak load. The plane is much larger than the plane of the mode- II shear plane and therefore requires even more energy for fracture initiation.

4.1.4 Sensitivity analysis of fracture properties of CPB to sulfate content

From the obtained data, it is clear the fracture properties of the CPB are influenced by the changes to internal sulfate concentration. The fracture properties of the CPB directly influence the fracture behavior of the CPB. Therefore, it is vital to evaluate each fracture properties level of sensitivity to internal sulfate content to aid in underground backfill technology application. Backfill operations may select which method of prediction to crack initiation they may choose, namely fracture toughness or energy to crack initiation (W_c) may be chosen to predict the CPB behavior. Therefore, the following discussion aims to provide further insight to the effect of internal sulfate concentration on the evolutive behavior of the fracture toughness and work to crack initiation of the CPB.

In order to evaluate sensitivity, there must be a conversion of the required data into comparable variables. Therefore, the 0ppm control CPB sample data may be used as the reference data to which the target data can be compared. This process is repeated at each curing time. Therefore, the sulfate concentration becomes the only factor affecting any changes in the material property of the CPB. The ratio of the change in the value of each property to the change in sulfate determines the variation of the variable. From which, the sensitivity index (SI) is determined from the following equation:

$$SI = \frac{1}{n \cdot m}\left\{\sum_{i=1}^{n}\sum_{j=1}^{m}\left[\left(\frac{q_{s_i\_t_j} - q^r_{s_0\_t_j}}{q^r_{s_0\_t_j}}\right)\Big/ s_i \times 100\%\right]\right\} \quad (4.1)$$

where $q_{s_i - t_j}$ represents the target fracture property q (i.e., material stiffness, fracture toughness, the energy of crack initiation, or energy of fiber bridging) at a sulfate content of s_i and a curing time of t_j, $q^r_{s_0 - t_j}$ denotes the reference value of fracture property from control FR-CPB without the addition of sulfate solution. It should be noted that four different sulfate contents (s_0=0ppm, s_1=5000ppm, s_2=15000ppm, and s_3=25000ppm) and four different curing times (t_1=3days, t_2=7days, t_3=28days, t_4=90days) were adopted in this study. Since the dataset corresponding to s_0=0ppm is used as the reference values (i.e., $q^r_{s_0 - t_j}$), n=3 and m=4 are set as the upper bounds of summation in Eq 4.1.

Figure 4.9 represents the different sensitivity values determined from the varying levels of sulfate concentration. In this study, the fracture energy is 0.516, 0.228, and 0.360 for mode-I, mode-II, and mode-III, respectively. However, while it can be seen in mode-I that the stiffness SI is very similar to the SI for mode-I fracture energy (0.521 and 0.516, respectively), the stiffness and fracture toughness SI is consistently lower than the SI for fracture energy in mode-II and mode-III. This indicates that fracture energy is more sensitive to internal changes in sulfate concentration than the material stiffness and fracture toughness.

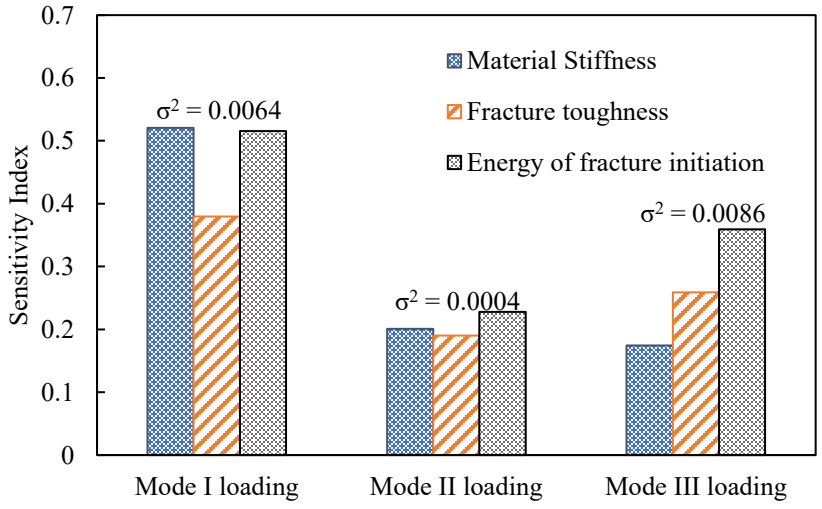

Figure 4.9. Sensitivity of fracture properties to sulfate content under different loading conditions.

As stated, fracture toughness and fracture energy have both been used in the engineered design of the CPB materials. However, when considering the safe engineered design of the CPB, the material stiffness is of practical importance. This is due to the fact that stiffness directly influences the CPB/rock interface, and a stiffer CPB mass will provide more immediate support to the surrounding rock body. It is beneficial to determine a more appropriate material property for the prediction of the mechanical behavior of the CPB as a fracture property that shows consistent evolution with stiffness can provide the most beneficial engineered design. The correlation factor (p) can be used to evaluate fracture property with material stiffness and can be used to evaluate material properties that vary with stiffness similarly.

$$\rho_{t_j} = \frac{\sum_{i=0}^{n}\left(q_{s_i\_t_j} - \overline{q_{t_j}}\right)\left(k_{s_i\_t_j} - \overline{k_{t_j}}\right)}{\sqrt{\sum_{i=0}^{n}\left(q_{s_i\_t_j} - \overline{q_{t_j}}\right)^2} \cdot \sqrt{\sum_{i=0}^{n}\left(k_{s_i\_t_j} - \overline{k_{t_j}}\right)^2}} \tag{4.2}$$

with:

$$\begin{cases} \overline{q_{t_j}} = \dfrac{1}{n+1}\sum_{i=0}^{n} q_{s_i\_t_j} \\ \overline{k_{t_j}} = \dfrac{1}{n+1}\sum_{i=0}^{n} k_{s_i\_t_j} \end{cases}$$

Where $\overline{q_{t_j}}$ and $\overline{k_{t_j}}$ respectively denote the average value of target fracture property (i.e., fracture toughness K and energy of crack initiation (W_c) and material stiffness with different sulfate content (s_i) at the same curing time (t_j). Since four different curing times were adopted, n=3 is set to the upper bounds of summation operation in Eq 4.2. To pinpoint the difference of fracture property with the correlation of material properties, the coefficient k and Wc are linked to other material properties at the same curing time and loading condition. In this way, sulfate becomes the sole factor changing the target data.

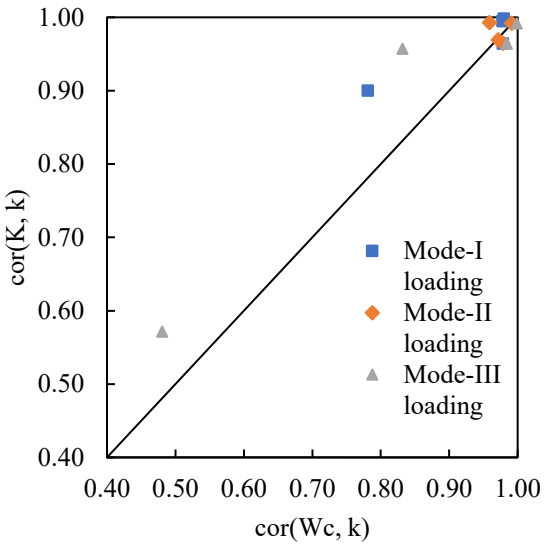

Figure 4.10. Comparison of correlation between target fracture property (K: fracture toughness, and Wc: energy of crack initiation) and material stiffness (k).

Figure 4.10 shows the plot correlation between fracture property and material stiffness. The value of the correlation coefficient is able to determine the comparative similarity between two separate sets of data. Therefore, the high correlation value found in the data set represents the high correlation of variation between fracture toughness and fracture energy with stiffness. From this figure, sulfate has a significant and consistent effect on the overall mechanical behavior and material properties of the CPB.

Additionally, it can be seen that there is a stronger correlation between fracture toughness and material stiffness (as more points lie above the 1:1 line). As the fracture toughness is determined from the peak force applied to the CPB, it is also a strength-related material property with stiffness; therefore, this relationship is logical. To assist in the design of CPB materials, fracture toughness may be used as a reliable tool in this regard instead of material stiffness. However, it should be noted that when deformation must be considered in the design of CPB materials, fracture energy (Wc) is the recommended approach as deformation information is included in the definition of fracture energy. Therefore, when deformation tolerance is crucial to the CPB design requirements, fracture energy must be the chosen material property used in the analysis.

4.2 Effect of sulfate content on fracture behavior and properties of FR-CPB

4.2.1 Effect of sulfate content on mode-I fracture behavior of FR-CPB

The results of the load-displacement behavior for mode-I FR-CPB loading are shown below in Figure 4.11. The results obtained show that, like CPB, the inclusion of sulfate has an impact on the mechanical behavior of the FR-CPB. As can be observed in the 3-day mode-I load-displacement results, high sulfate content results in a lower pre-peak slope, lower peak, and reduced post-peak load-displacement behavior of the 15000ppm and 25000ppm sulfate FR-CPB respectively. As the majority of strength is related to the development of CSH and CH within the pore space of the CPB, when excess sulfate is introduced within the fresh paste, the excess sulfate ion consumes the CH while rapidly generating expansive phases reducing the performance of the CPB in the early ages of development. Additionally, the development of the gypsum may contribute to the production of ettringite development due to further reactions with the C_3A and C_4AF components of Portland cement. The expansive phases in themselves provide no additional strength to the FR-CPB matrix. As with fibreless CPB, the FR-CPB exhibits continual improvement in load-displacement behavior after 7 days of development, and the effects of sulfate inclusion become more obvious as curing time progresses. The improvement in mechanical behavior extends into the post-peak phases of the load-displacement curve. The development of expansive phases of gypsum and ettringite is confined within the pore space of the FR-CPB due to the stiff plastic containment mold. When the cement cures, the internal cured matrix locks the expansive phases within the pore space resulting in a densified structure. This increase in densification leads to stronger bond strength between the CPB matrix and the polypropylene fibers resulting in improved post-peak load-displacement behavior in the FR-CPB with sulfate compared to control 0ppm FR-CPB. As curing time increases, the passive confinement the FR-CPB experiences further lock the expansive phases into the pore space of the FR-CPB. When the CPB cylinder is removed, the locking of the matrix cannot be released, resulting in improved load-displacement behavior.

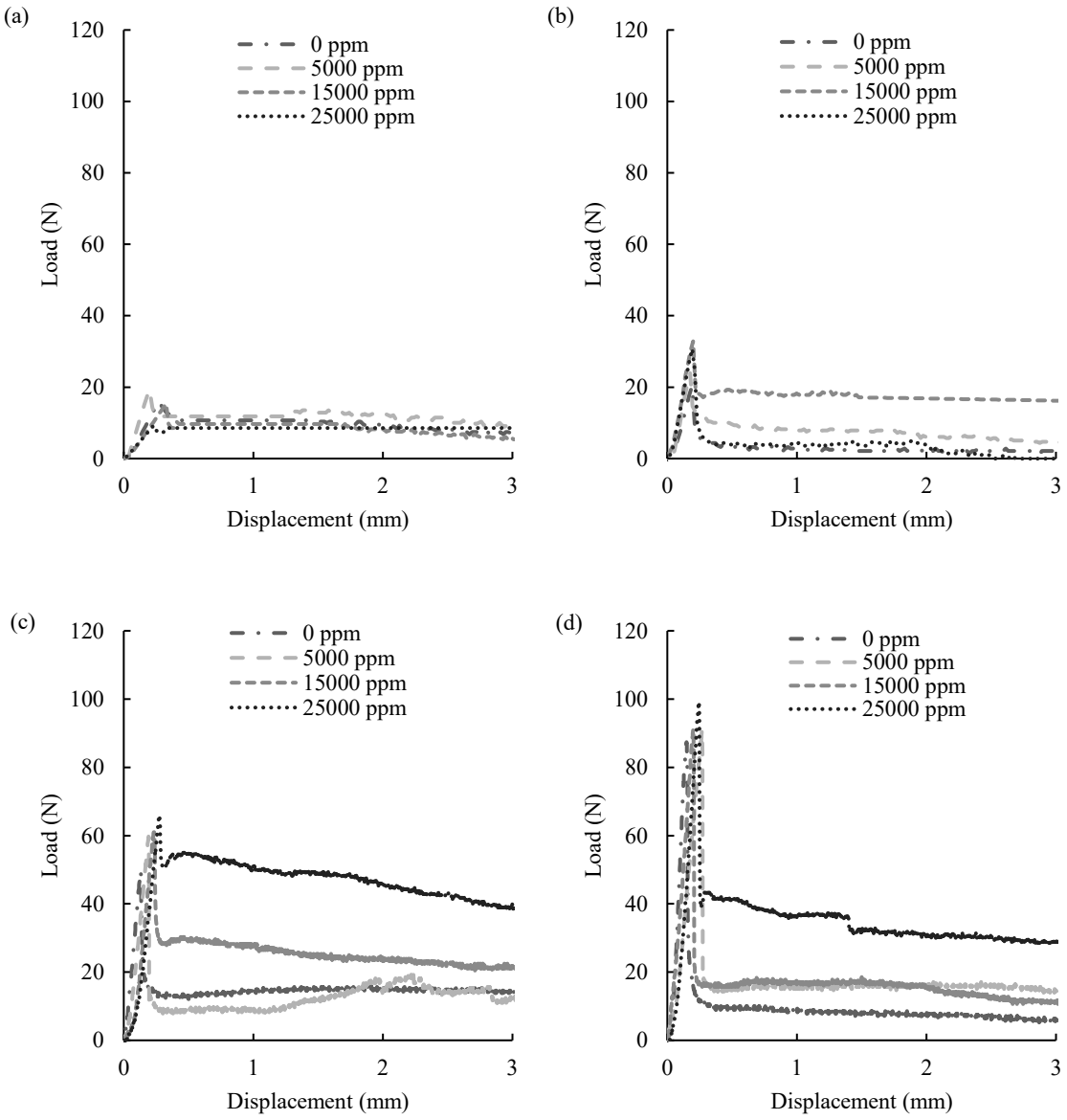

Figure 4.11. Effect of sulfate content on the mode-I load-displacement behavior at (a) 3 days, (b) 7 days, (c) 28 days, and (d) 90 days.

4.2.2 Effect of sulfate content on mode-II fracture behavior of FR-CPB

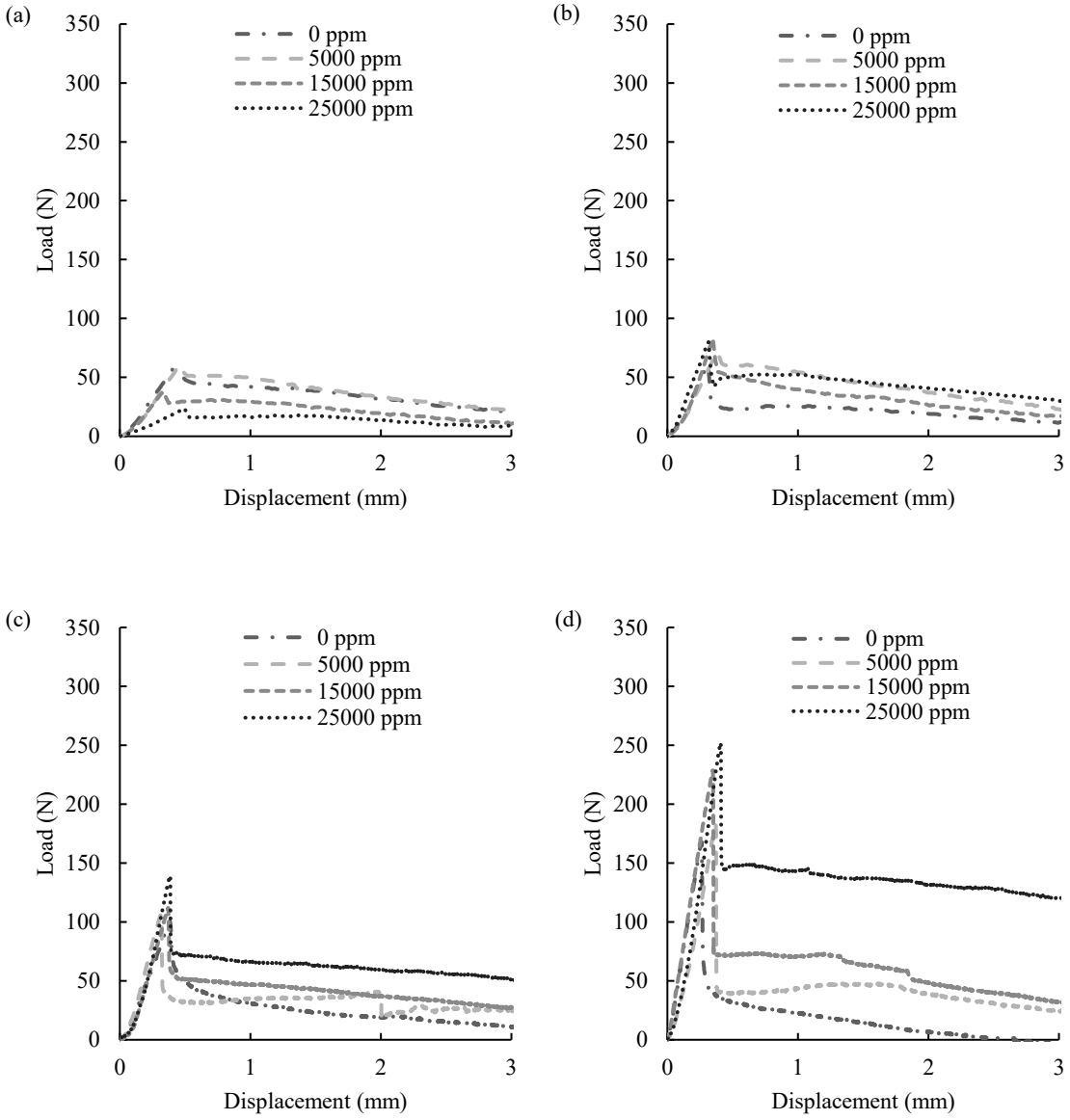

Figure 4.12. Effect of sulfate content on the mode-II load-displacement behavior at (a) 3 days, (b) 7 days, (c) 28 days, and (d) 90 days.

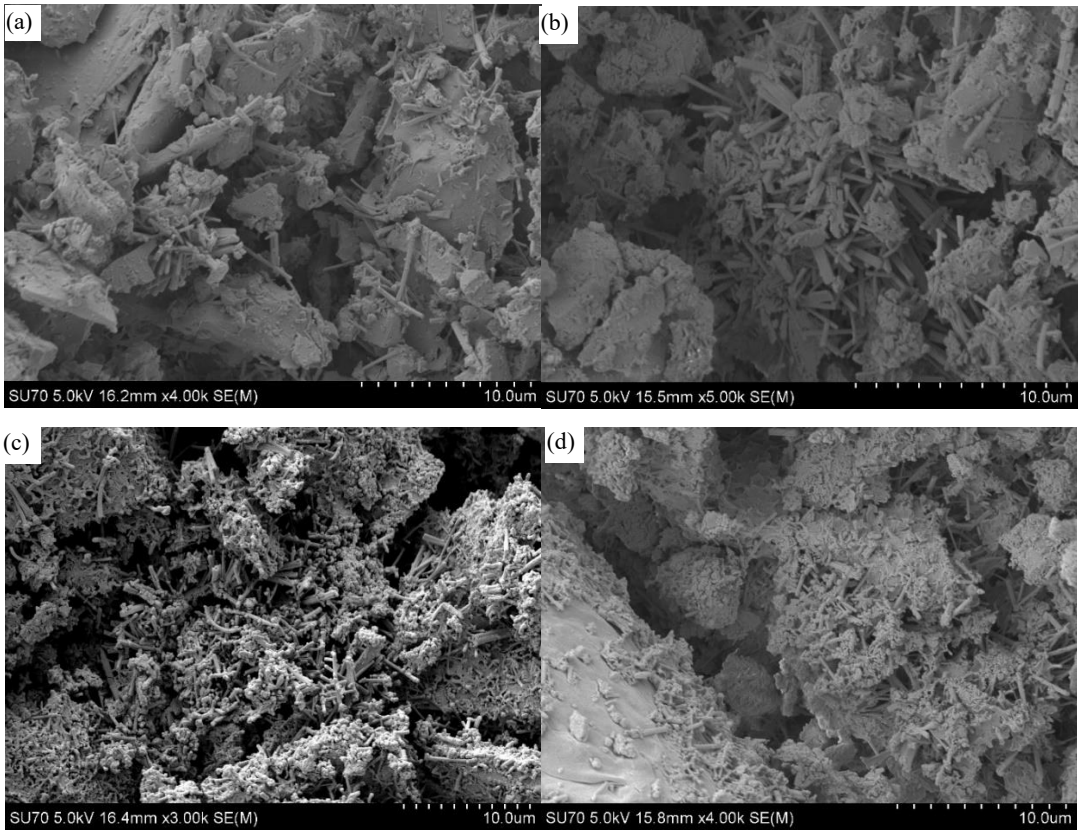

Figure 4.13. SEM images of FR-CPB matrix with sulfate concentration of 25000ppm at (a) 3 days, (b) 7 days, (c) 28 days, and (d) 90 days.

Figure 4.12 shows the mode-II load-displacement behavior of the FR-CPB at various sulfate concentrations and curing times. At this age, it can be observed that the sulfate has a detrimental effect on the pre-peak behavior of the FR-CPB. Due to the pre-peak behavior of cementitious materials being predominantly reliant on the inner matrix of the CPB, it is evident that the existence of sulfate affects the evolutive strength development of CPB. Similar to mode-I FR-CPB load-displacement behavior, after 3 days there is a clear improvement in mode-II load-displacement behavior in the FR-CPB containing sulfate beyond the control 0ppm FR-CPB. The improvement is not only applicable to the pre-peak and peak load behavior but can also be seen in the post-peak behavior of the FR-CPB. Under mode-II loading, a friction surface is created along the crack plane that resists the continued post-peak fracture simultaneously with the effect of the fibers. This greatly enhances the resistance to continued fracturing in the mode-II configuration. This post-peak improvement that is observed into the advanced age of the FR-CPB further confirms that the expansive phase development occurring within the sulfated FR-CPB samples is improving the matrix fiber interaction, and it is this mechanism that is improving the post-peak resistance. As

shown in Figure 4.13, more expansive phases can be detected in the microstructure of the FR-CPB as the curing time increases. As the expansive phases continue to hydrate, the pore water is consumed to a greater extent within the CPB matrix. Therefore, the interparticle friction is enhanced even further as curing time increases.

4.2.3 Effect of sulfate content on mode-III fracture behavior of FR-CPB

When the FR-CPB is placed within the underground stope, the surrounding rock interacts with the FR-CPB body. The jagged structure of the rock wall can create a "wall effect" in which a coarsened matrix is developed at the rock/CPB boundary. When the mining operation continues, the rock may be removed, exposing the coarsened FR-CPB boundary layer. Subject to the unconfined biaxial loading conditions, shearing may occur within the body of the FR-CPB. The tearing loads developed will propagate cracks through the FR-CPB. Therefore, examining the mode-III out-of-plane shear is essential to developing a complete understanding of the behavior of the FR-CPB. The behavior examined for the FR-CPB subjected to mode-III loading is unique compared to the behavior of the CPB and the mode-I and mode-II FR-CPB. When subjected to mode-III loading, the FR-CPB exhibits pseudo-hardening behavior, which can be observed in Figure 4.14. This observation indicates that there is a stronger fiber interaction occurring during torsional loading when compared to mode-II in-plane shearing. The additional fiber interaction is a result of the fiber rotation required when subjected to mode-III loading. As the CPB cracks, the rough surface generated between the two surfaces will generate friction between the particle surfaces. However, the fibers must also pull and rotate from the original anchorage point. This mechanism requires the CPB to be re-arranged by the polypropylene fibers as soon as the fracture surface is formed. For this reason, the load required to continue fracturing the CPB in the mode-III configuration requires additional energy.

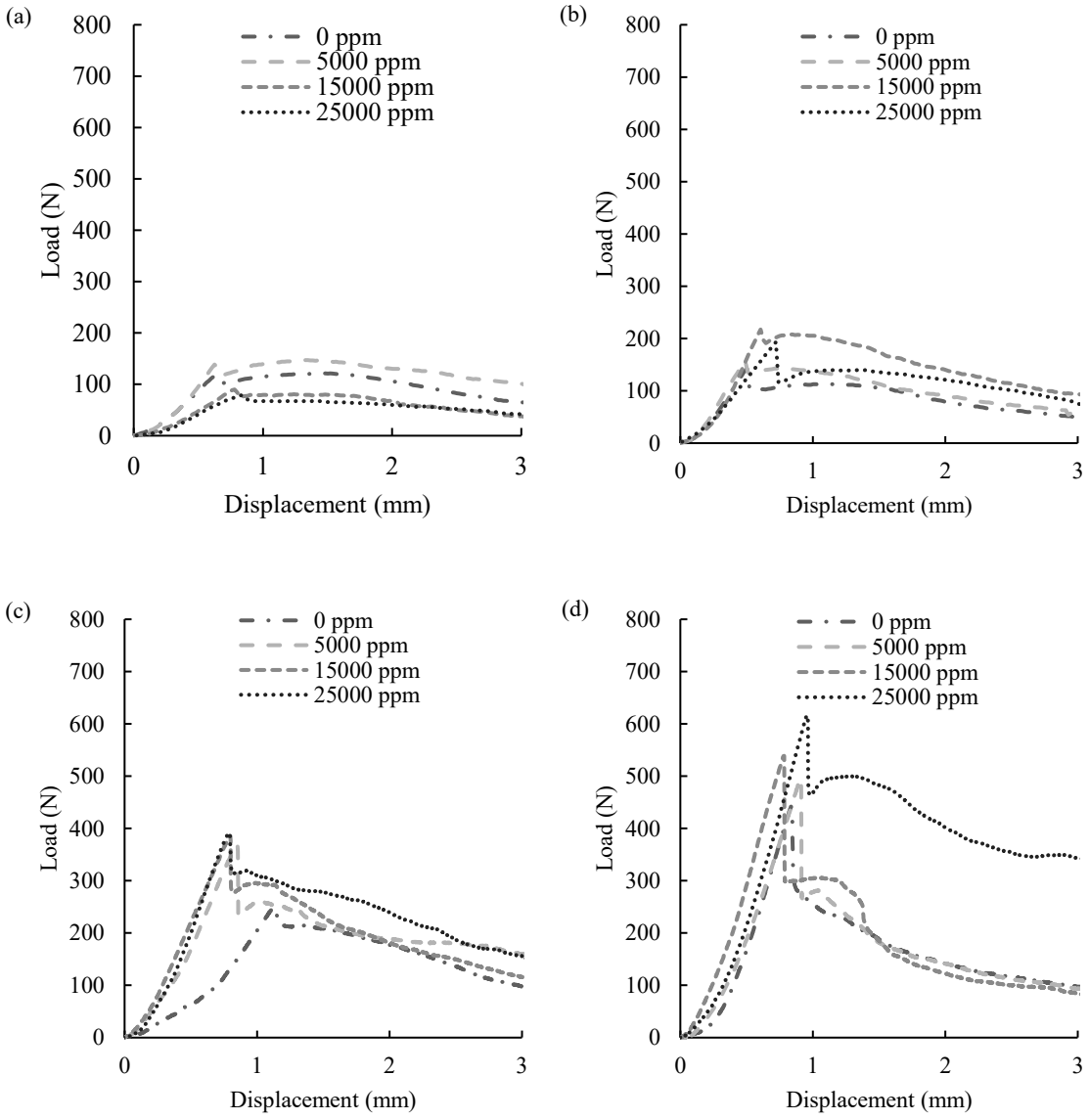

Figure 4.14. Effect of sulfate content on the mode-III load-displacement behavior at (a) 3 days, (b) 7 days, (c) 28 days, and (d) 90 days.

4.2.4 Effect of sulfate content on fracture properties of FR-CPB

4.2.4.1 Effect of sulfate content on material stiffness of FR-CPB

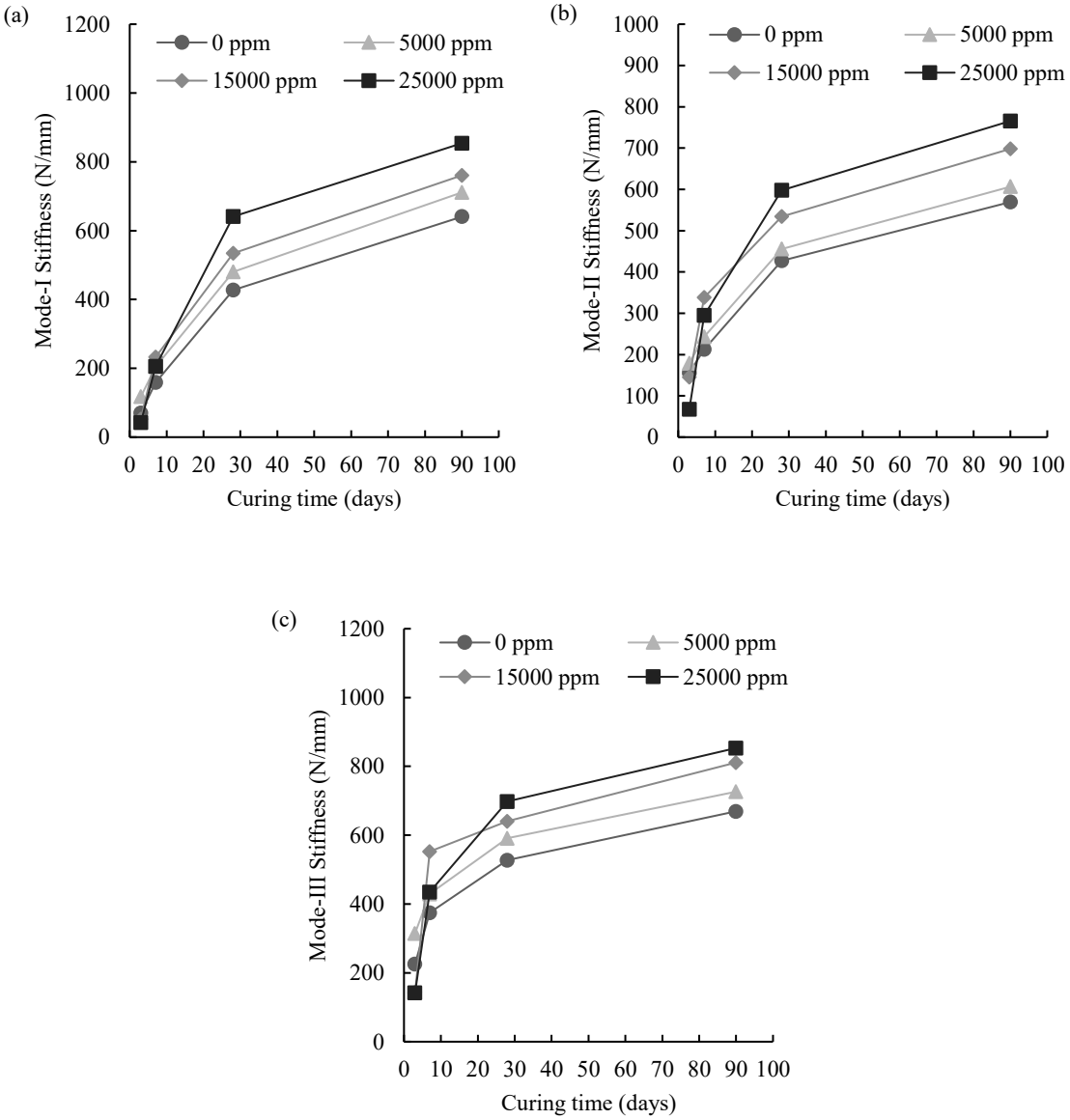

Figure 4.15. Effect of sulfate content on the material stiffness of FR-CPB in (a) mode-I, (b) mode-II, and (c) mode-III.

As shown in Figure 4.15, the FR-CPB continuously improves with increases in sulfate content. It is important to note that the inclusion of fibers provides very limited improvement to the pre-peak load stiffness of the FR-CPB. Therefore, the stiffness of the FR-CPB shows very similar evolutive behavior when compared to the CPB. The enhancement of material stiffness corresponds to a densified bulk matrix of the FR-CPB. In the mode-II and mode-III configurations a non-linear

increase in material stiffness is observed. As mode-I fracture behavior is solely a function of tensile fracture behavior, the increase in material stiffness in mode-II and mode-III can be attributed to the increased particle friction experienced by the FR-CPB with internal sulfate content. The inclusion of high levels of sulfate within the FR-CPB promotes the generation of gypsum and ettringite. The expansive phase development consumes pore water greatly increasing the interparticle friction. As a result, the stiffness is increased to a higher degree when measuring mode-II and mode-III material stiffness when compared solely to mode-I FR-CPB stiffness.

4.2.4.2 Effect of sulfate content on fracture toughness of FR-CPB

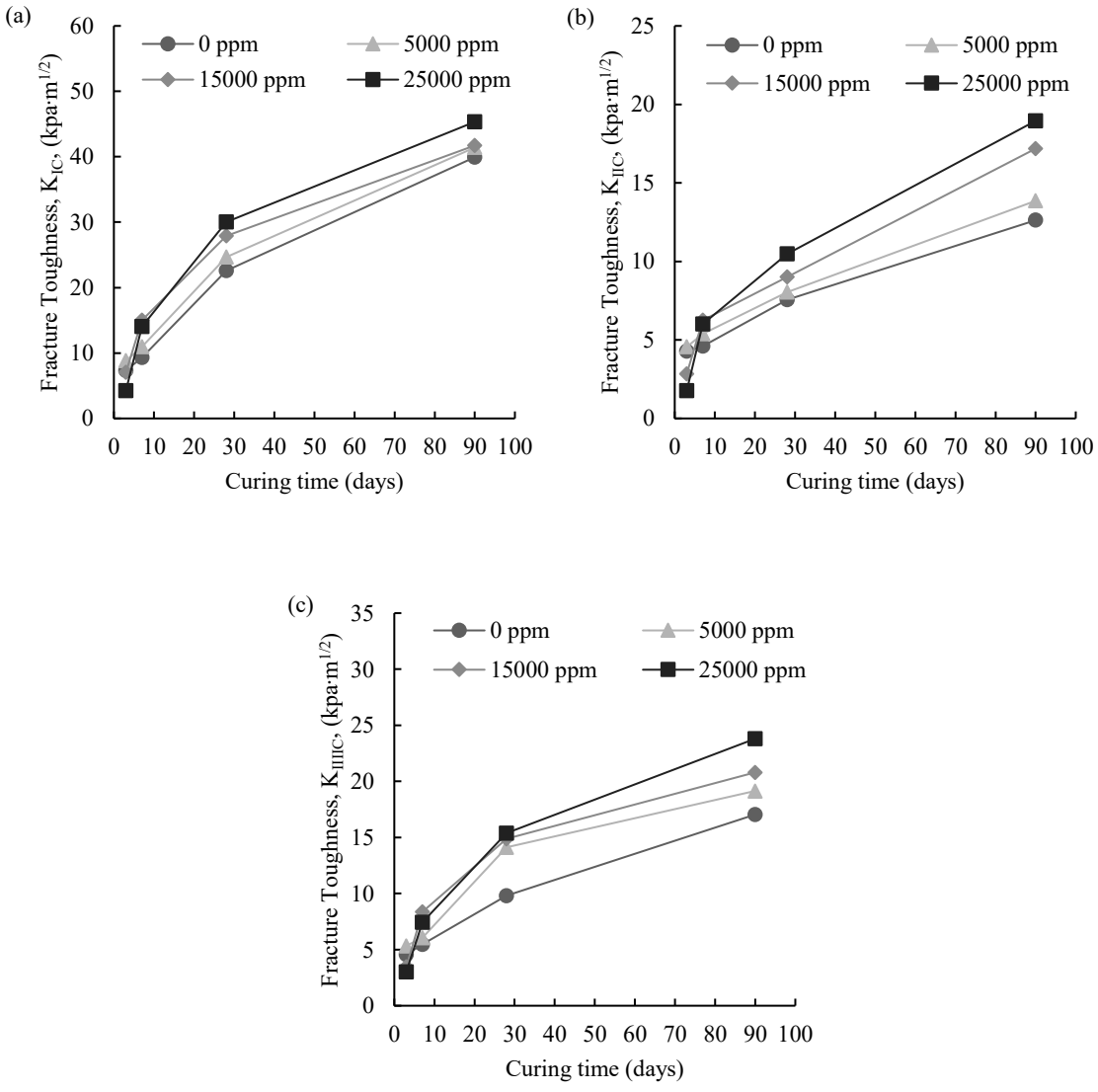

Figure 4.16. Effect of sulfate content on the evolutive fracture toughness of FR-CPB under (a) mode-I, (b) mode-II, and (c) mode-III loadings.

Figure 4.16 shows the improvement of fracture toughness with the increase of sulfate content in mode-I, mode-II, and mode-III loadings. The formation of the expansive phases within the FR-CPB increases the passive confinement pressure resulting in a denser microstructure in the FR-CPB. As fracture toughness is a strength-related material property, as the density increases, undoubtedly there will be an effect on the fracture toughness of the FR-CPB. In Figure 4.16, it is clear that the samples with sulfate inclusion have a higher resulting fracture toughness in advanced-age FR-CPB when compared to the control 0ppm FR-CPB. Beyond the fracture toughness values, the relationship between the measured fracture toughness is of great importance. By investigating such relationships, insight into the reliable estimation of mode-II and mode-III fracture toughness may be garnered. This is beneficial as the measurement of the shear fracture behavior and preparation of the samples is inherently more complicated than the comparative preparation and measurement of the mode-I fracture behavior. Figure 4.17 below shows the relationship between mode-II and mode-I (K_{IIC}/K_{IC}) and mode-III and mode-I (K_{IIIC}/K_{IC}) fracture toughness. It can be observed in the figure that the fracture toughness ratios have limited dependence on internal sulfate content; therefore, the mode-I fracture toughness measurement may be used as a reliable quantity to estimate the mode-II and mode-III fracture toughness values.

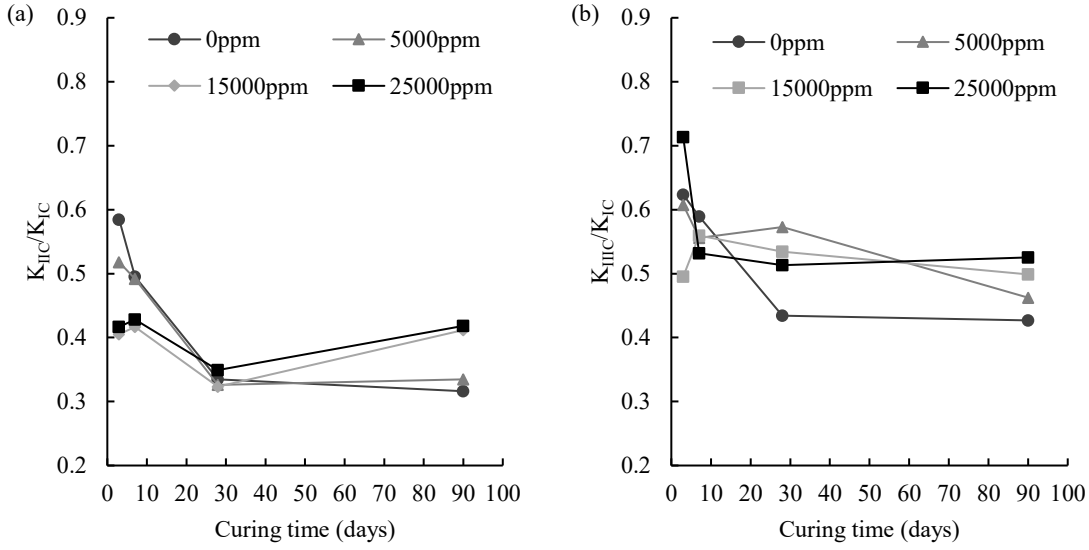

Figure 4.17. Comparison of fracture toughness ratios for FR-CPB: (a) K_{IIC}/K_{IC} and (b) K_{IIIC}/K_{IC}

4.2.4.3 Effect of sulfate content on fracture energy of FR-CPB

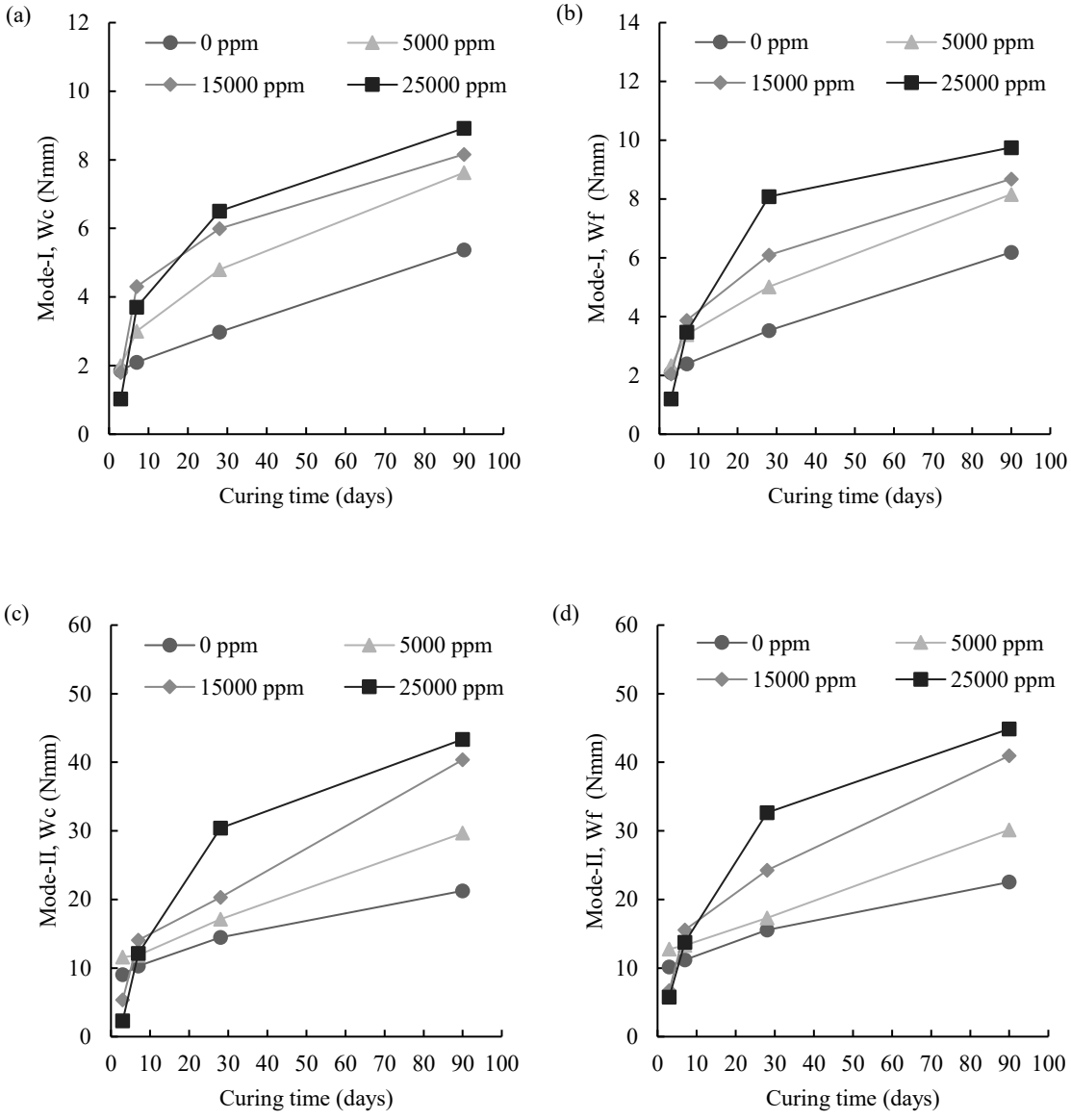

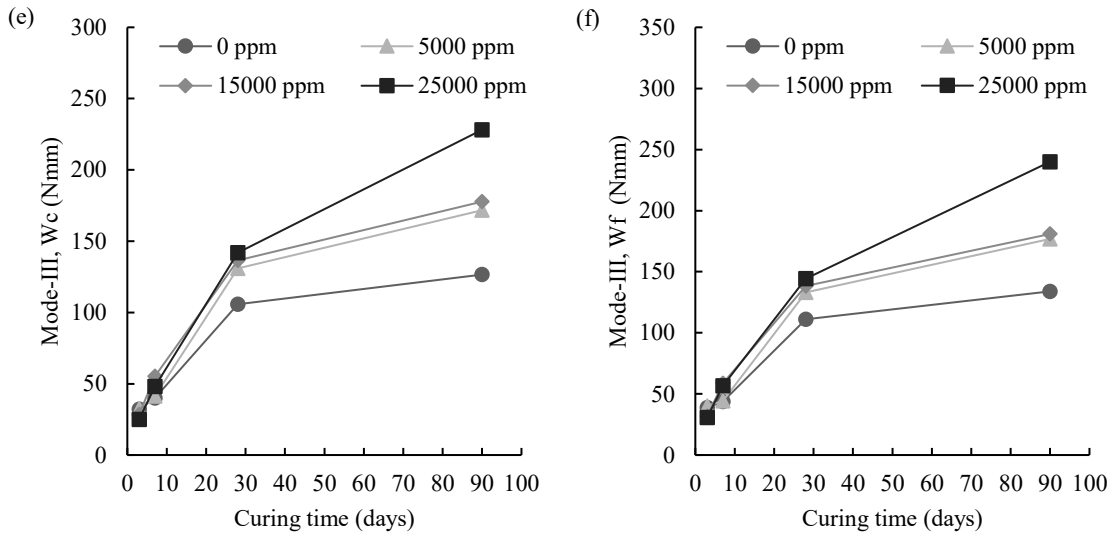

Figure 4.18. Effect of sulfate content on the evolutive energy to crack initiation (Wc) and energy of fiber bridging (Wf) under mode-I (a and b), mode-II (c and d), and mode-III (e and f) loading.

Figure 4.18 shows the evolution of fracture energy with respect to sulfate concentration and curing time. As can be seen in the figure, the magnitude of fracture energy is sensitive to the changes in sulfate content, especially at later ages. FR-CPB with a higher sulfate content is able to dissipate more strain energy at advanced ages and, thus, further resist the crack onset and growth in the matrix. This trend is shown consistently across the three modes tested in the experimental study. As the expansive phases continue to develop, the increase in fracture energy can be attributed to the consequences of this internal material evolution. Namely, as stated in the previous section mode-I fracture behavior is dominated by interparticle cohesion. The cohesion of cementitious materials is directly related to the cement hydration reactions. As the expansive phases continue to develop, the pressure within the mold increases, driving densification between the cementitious CSH gel resulting in improved mode-I material properties and increased fracture energy requirement as the curing time increases. As for mode-II, cohesion and friction play a role in the magnitude of fracture energy dissipation. As expansive phase development continues, not only does the increased pressure improve cementitious bonding, interparticle friction plays a role in the fracture energy required to propagate cracks through the FR-CPB, as the fracture surface must slide in the plane in order for this mechanism to occur. The mechanism for mode-III is similar to mode-II; however, in the experimental testing configuration for this study, the cracking plane surface where cementitious bonds are broken is much greater than the mode-II configuration.

Additionally, the friction surface along this cracking plane is much greater in mode-III when compared to mode-II. Both of these factors contribute to the large increase in fracture energy of the FR-CPB.

Comparison across the modes shows the energy to crack initiation (W_c) and the energy of fiber bridging (W_f) increase from mode-I to mode-II and to mode-III. The energy of fiber bridging is consistently greater than the energy of crack initiation. The obtained results indicate that additional external work is required to fully activate the fiber reinforcement in the CPB matrix after the onset of crack initiation. It is important to note that the mechanism observed for all FR-CPB was fiber pull-out, and no fiber rupture was observed throughout the testing program. This indicates that the interfacial bond between CPB and fiber is not strong enough to overcome the polypropylene fiber strength. The improved energy of fiber bridging is a result of the refined pore structure resulting from the increased expansive phases development. As the expansive gypsum and ettringite form, the increased pressure in the cylindrical mold densifies the FR-CPB bulk matrix. This increases the interfacial bond between the cementitious material and the polypropylene fibers. Therefore, as the strain energy is initially released, more energy is required to transition from the load predominantly supported by the CPB bulk matrix to the fibers fully supporting the externally applied load.

4.2.4 Sensitivity analysis of fracture properties of FR-CPB to sulfate content

Based on the obtained results, it can be found that the fracture properties of FR-CPB are sensitive to the changes in sulfate content. Since the fracture properties materials are intimately related to the fracture behavior and thus the in-situ performance of mine backfill technology, it is of practical importance to evaluate the degree of sensitivity of each fracture property to the sulfate content. Moreover, both fracture toughness and energy of crack initiation (W_c) can be adopted to predict the onset of the crack in the CPB matrix. It is of great significance to identify the difference between fracture toughness and fracture energy in terms of engineering application. The present discussion aims to address these two questions and provides a deep insight into the effect of sulfate content on the evolution of fracture properties of FR-CPB materials. To evaluate the sensitivity of fracture toughness to the sulfate content, the prerequisite is to convert the target data into dimensionless and comparable variables. In this regard, the dataset obtained from control FR-CPB with different sulfate contents can be used as reference values. Then, the relative change in each

fracture property can be calculated with reference to the counterpart of control FR-CPB at the same curing time. Since the relative change is determined at the same curing time, the sulfate content becomes the dominant factor affecting the magnitude of relative changes. Therefore, the ratio between the relative change of each fracture property and the change in sulfate content can be determined to evaluate the variation of the dimensionless variable per unit change in sulfate change (i.e., the absolute sensitivity). After that, the global sensitivity index (SI) can be obtained through the average operation of absolute sensitivity through the following equation:

$$SI = \frac{1}{n \cdot m}\left\{\sum_{i=1}^{n}\sum_{j=1}^{m}\left[\left(\frac{q_{s_i\_t_j} - q^r_{s_0\_t_j}}{q^r_{s_0\_t_j}}\right)\Big/ s_i \times 100\%\right]\right\} \tag{4.3}$$

where $q_{s_i - t_j}$represents the target fracture property q (i.e., material stiffness, fracture toughness, the energy of crack initiation, or energy of fiber bridging) at a sulfate content of s_i and a curing time of t_j, $q^r_{s_0 - t_j}$ denotes the reference value of fracture property from control FR-CPB without the addition of sulfate solution. It should be noted that four different sulfate contents (s_0=0ppm, s_1=5000ppm, s_2=15000ppm, and s_3=25000ppm) and four different curing times (t_1=3days, t_2=7days, t_3=28days, t_4=90days) were adopted in this study. Since the dataset corresponding to s_0=0ppm is used as the reference values (i.e., $q^r_{s_0 - t_j}$), n=3 and m=4 are set as the upper bounds of summation in Eq. 4.3.

As shown in Figure 4.19, the fracture properties demonstrate different sensitivity to the sulfate content. Precisely, the SI of fracture energy is in the range of 0.3 to 0.47, while the SI associated with stiffness and fracture toughness is consistently less than 0.26 under mode I and mode II loading. The obtained SI value implies that fracture energy is more sensitive to the sulfate content under mode-I and mode-II loading. This is because the combined effect of sulfate-induced volume expansion and locked confinement can enhance the fiber-matrix interaction and thus dissipate a greater amount of strain energy with the increase of sulfate content. Consequently, fracture energy is highly sensitive to the changes in sulfate content. However, it is interesting to find that the fracture properties show a very limited discrepancy in SI under mode-III loading, which can be evidenced by the small variance (σ^2=0.001) of SI data corresponding to the mode-III loading. In other words, the sensitivity of fracture energy to sulfate content becomes weaker under mode-III loading compared with the counterparts under mode-I and mode-II loadings. The weakened

sensitivity of mode-III fracture energy can be explained by the contribution of the fiber rotation around the anchor points along the crack surfaces to fracture energy. The obvious pseudo-hardening behavior indicates that the fiber-crack surface interaction makes a greater contribution to the development of fracture energy. It should be pointed out that the additional fiber-crack surface interaction is governed by the fiber-crack surface friction and thus insensitive to the changes in chemical factors. Consequently, a reduced SI was obtained from fracture energy under mode-III loading.

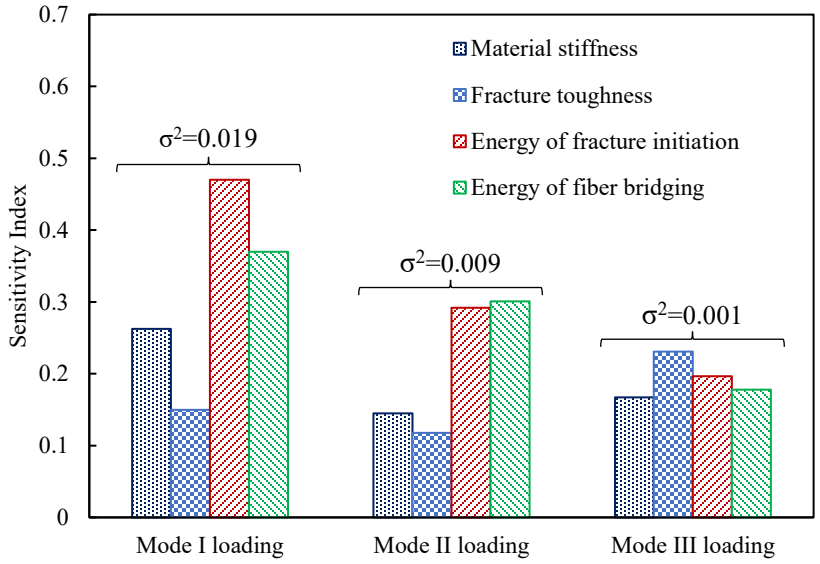

Figure 4.19. Sensitivity of fracture properties to sulfate content under different loading conditions.

Moreover, both fracture toughness and energy of crack initiation (W_c) have been employed in the engineering design of cementitious composite. It is essential to identify the more appropriate quantity for the evaluation of the mechanical behavior of CPB materials. Since hardened CPB mass is required to provide reliable ground support to the surrounding rock, the safe engineering design of the CPB structure requires full consideration of rock/CPB interaction. In this regard, material stiffness and material deformation tolerance are two major concerns to the stability of CPB and rock mass. For the material stiffness, a stiffer mine backfill body is able to provide more effective immediate support to surrounding rock mass, which cannot only maintain the integrity of surrounding rock mass, but also restrict the land subsidence. In other words, a larger material stiffness is practically desirable. Correspondingly, the fracture property, which shows a more consistent evolution with material stiffness, is more suitable for the engineering design of CPB

materials. This is because when such a fracture property is designed to a higher value, the material stiffness can be improved to a greater extent simultaneously. Therefore, the correlation (ρ) of fracture property and material stiffness can be used to evaluate the degree to which the target data vary similarly.

$$\rho_{t_j} = \frac{\sum_{i=0}^{n}\left(q_{s_i\_t_j} - \overline{q_{t_j}}\right)\left(k_{s_i\_t_j} - \overline{k_{t_j}}\right)}{\sqrt{\sum_{i=0}^{n}\left(q_{s_i\_t_j} - \overline{q_{t_j}}\right)^2} \cdot \sqrt{\sum_{i=0}^{n}\left(k_{s_i\_t_j} - \overline{k_{t_j}}\right)^2}} \tag{4.4}$$

with:

$$\begin{cases} \overline{q_{t_j}} = \dfrac{1}{n+1}\sum_{i=0}^{n} q_{s_i\_t_j} \\ \overline{k_{t_j}} = \dfrac{1}{n+1}\sum_{i=0}^{n} k_{s_i\_t_j} \end{cases}$$

where $\overline{q_{t_j}}$ and $\overline{k_{t_j}}$ respectively denote the average value of target fracture property (i.e., fracture toughness K and energy of crack initiation (W_c) and material stiffness with different sulfate content (s_i) at the same curing time (t_j). Since four different curing times were adopted, n=3 is set to the upper bounds of summation operation in Eq. 4.4. To identify the discrepancy of fracture property in the correlation with material properties, the obtained correlation coefficient of k and Wc are respectively paired with the counterparts of material properties at the same curing time and same loading conditions. It should be noted that the correlation ρ_{tj} is determined through target data at the same curing time (t_j). Therefore, the sulfate content becomes the dominant factor responsible for the changes in the target data under different loading conditions.

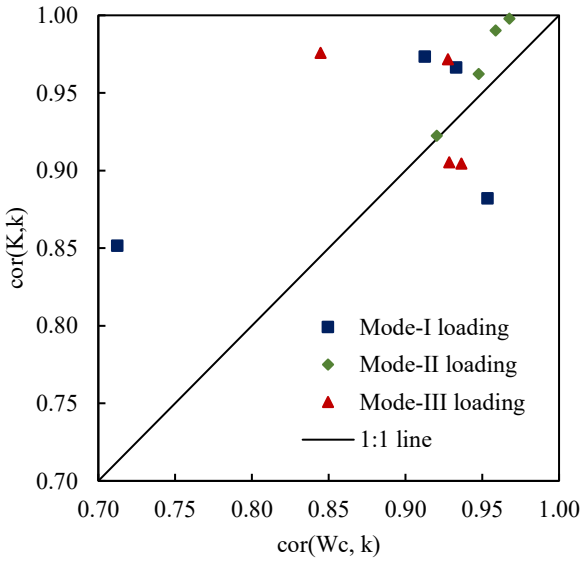

Figure 4.20. Comparison of correlation between target fracture property (K: fracture toughness, and Wc: energy of crack initiation) and material stiffness (k).

The comparison of the correlation coefficient between target fracture property and material stiffness is plotted in Figure 4.20. It can be found that all correlation coefficients are greater than 0.7. Since the correlation coefficient is a type of normalized covariance and does not depend on the absolute values of fracture properties. The values of the correlation coefficient are able to evaluate the degree of correlation between two different datasets. Therefore, the higher correlation values indicate that the variation of both fracture toughness (K) and energy of crack initiation (W_c) are strongly correlated to that of the material stiffness under different loading conditions. Such results quantitatively confirm that sulfate content can impose a significant and relatively consistent impact on all fracture properties. Moreover, the majority of data points are located above the 1:1 line, which implies that fracture toughness shows a stronger correlation with material stiffness. Such results are consistent with the conventional findings of the strength-related properties. It is well known that material strength such as compressive, tensile, and shear strength shows a highly positive correlation with material stiffness. The fracture toughness is determined through peak force and thus is a type of strength-related property as well. Therefore, when immediate ground support to the surrounding rock mass is the main concern, in practice, fracture toughness can be used as a more reliable fracture property to guide the design of CPB materials under different loading conditions. However, it should also be pointed out that the deformation information is

integrated into the determination of W_c. Therefore, the W_c is highly recommended in the engineering design of CPB when the deformation tolerance of backfill materials is the main concern under the finite deformation of the rock mass.

Chapter 5 Conclusions and recommendations

5.1 Conclusions

To investigate the effect of sulfate content on the fracture behavior and material properties of CPB and FR-CPB, a comprehensive experimental testing program was designed and conducted in the present study. CPB and FR-CPB were prepared with various sulfate concentrations, including 0, 5000, 15000, and 25000ppm, and cured at different curing times (3, 7, 28, and 90 days). By conducting SCB (to capture the mode-I and mode-II fracture behaviors) and ENDB (to capture the mode-III fracture) tests integrated with auxiliary analysis (SEM observation and dry density measurement), a thorough understanding of the microstructure and macroscale fracture behavior and properties of FR-CPB materials is garnered. From the conducted study, the following conclusions have been drawn:

1. Internal sulfate can significantly affect the pre-peak and peak behavior of the CPB and FR-CPB subjected to mode-I, mode-II, and mode-III loading at both early and advanced ages. In 3-day early-age CPB, the pre-peak behavior is reduced significantly in CPB and FR-CPB subjected to 15000 and 25000ppm internal sulfate content. Compared to the 0ppm control CPB, the slopes are much shallower, and the peak load achieved is significantly lower in the high sulfate content CPB.
2. The CPB and FR-CPB not only exhibit this behavior but also show that the post-peak behavior of the CPB/FR-CPB is significantly lower when compared to the control material. This behavior is a result of the rapid formation of expansive phases of gypsum and ettringite formed within the CPB/FR-CPB mixture combined with the additional consumption of portlandite (CH), a strength contributing product of CPB, that occurs with excess sulfate present in the material mixture. This behavior is observed in mode-I, mode-II, and mode-III fracture loading configurations of the material.
3. At a 7-day curation time, there is a significant improvement in the pre-peak, peak, and post-peak fracture behavior of the high sulfate content 15000 and 25000ppm material. By 28 days, the high sulfate content CPB and FR-CPB shows much higher values when observing the pre-peak, peak, and post-peak behavior. This trend continues until the maximum curation time observed in the study at 90 days.

4. The observed behavior is a result of the curation conditions placed upon the material throughout the study to mimic true underground mining backfill conditions. When placed into the stiff plastic molds, the expansive phases and the typical hydration products are forced to form simultaneously in a limited volume. The production of excess expansive phases in the limited volume increases the confining pressure within the plastic mold. This, in turn, forces the hydration products into a tighter configuration, as evidenced by the increased dry density in the sulfated CPB and FR-CPB.
5. The increased densification as curing time increases is also confirmed by the SEM analysis. By observing the 25000ppm CPB and FR-CPB at 3, 7, 28, and 90 days there is clearly formation of expansive phases that remain into the advanced age stages of curing time. By examining the measurement scale of the CPB/FR-CPB, there are more hydration products at a smaller distance in the advanced-age CPB/FR-CPB when compared to the early age material.
6. The increased densification of the matrix is locked in place once curing has progressed and cannot be released by the removal of the CPB and FR-CPB from the plastic molds. The increases in density translate to the improvement of the load-displacement behavior of the CPB/FR-CPB. As there is a tighter interfacial bond between the hydration products and the polypropylene fiber, there is an increase in the load required to completely fracture the FR-CPB after the peak load has been achieved.
7. In the mode-III load-displacement behavior of the FR-CPB pseudo-hardening effect is observed in the post-peak behavior of the advanced age FR-CPB. This post-peak behavior is a result of the torsional out-of-plane fracture configuration not only being resisted by the polypropylene fibers but the additional particle rearrangement behavior that must occur to fracture the FR-CPB in the mode-III configuration. This behavior is less noticeable in the early age FR-CPB as the energy required to rearrange the particles during the torsional fracture is much less when compared to the advanced age FR-CPB.
8. Sulfate content affects the early and advanced age material properties in terms of stiffness, fracture toughness, work to crack initiation, and work of fiber bridging of the CPB and FR-CPB. In the early age material, increased sulfate content reduces the material stiffness, fracture toughness, work to crack initiation, and work of fiber bridging of the CPB/FR-

CPB. However, at advanced ages, sulfate improved the material properties of the CPB/FR-CPB.

9. Sensitivity analysis conducted on the CPB showed that fracture energy is more sensitive to internal changes in sulfate content than stiffness or fracture toughness. Additionally, the fracture toughness and stiffness showed a higher correlation compared to stiffness and energy of fracture. Fracture toughness was also observed to be highly correlated with stiffness as sulfate content is altered for FR-CPB.

All the established objectives outlined prior to the commencement of the research have been accomplished with regard to the investigation of the effect of internal sulfate on the fracture behavior and material properties of CPB and FR-CPB. The results from this study show internal sulfate has a profound effect on both the early and advanced age CPB and FR-CPB; therefore, this study contributes to the growing body of knowledge regarding cemented paste backfills and, the experimental results and analysis found in this study can improve the current methods of backfilling used in the mining industry. Additionally, from the obtained results and analysis of the effect of internal sulfate on the fracture behavior and material properties of CPB and FR-CPB, there is an increased ability to predict at what sulfate concentration (to 25000ppm) and curing time (to 90 days) you may have maximum or minimum resistance to fracture propagation and deformation from surrounding rock and you may plan mining operations using such information.

5.2 Recommendations for future work

Although extensive previous research, experimental testing, and result analysis were conducted to investigate the effect of internal sulfate on CPB and FR-CPB there are still many areas of study regarding CPB and FR-CPB with internal sulfate inclusion. Therefore, the following section aims to guide future researchers to further their studies in this field of work. Areas of future work regarding backfill technology, as determined by the author, are as follows:

1. Typical studies regarding sulfate on cementitious materials reference sulfate attack. Namely, when exposed to sulfate, there is the degradation of the behavior and material properties of the material. In this study, it was found that although high levels of sulfate reduce early age results, the advanced age results showed an improvement in the CPB and

FR-CPB behavior with the inclusion of sulfate. In CPB-type materials, there is a possibility that there is a higher requirement for sulfate concentration to induce the sulfate attack in the material. Future work may investigate higher levels of sulfate concentration (greater than 25000ppm) to determine at what concentration there is a degradation in material performance.

2. As expansive phase products are produced, there is a pore water consumption that occurs during this process. The hydration rates and water consumption within the CPB can be extremely complex. Therefore, instrumentation and monitoring of the internal water consumption, matric suction, and electrical activity may provide even further insight to the behavior and performance of the CPB, especially at early ages.
3. Development of mathematical modeling incorporating cement content, water to cement ratio, internal sulfate, and fiber inclusion to further investigate relationships between these constituents of CPB and FR-CPB, and confirm the results obtained in this study.
4. Once reliable mathematical modeling is achieved, applying complex loading conditions and confirming results with experimental data is highly recommended. This is due to true mining conditions involving complex loading conditions often difficult to test in laboratory settings.
5. Further investigate mode-I, mode-II, and mode-III fracture behavior and material properties of FR-CPB with varying levels of internal sulfate at different curing times using different types of fibrous material or fibrous material at different quantities.

References

Aldhafeeri, Z., & Fall, M. (2017). Sulphate induced changes in the reactivity of cemented tailings backfill. *International Journal of Mineral Processing*, *166*: 13–23. https://doi.org/10.1016/j.minpro.2017.06.007.

Andrade Neto, J. da S., De la Torre, A. G., & Kirchheim, A. P. (2021). Effects of sulfates on the hydration of Portland cement – A review. *Construction and Building Materials*, *279*. https://doi.org/10.1016/j.conbuildmat.2021.122428.

Benzaazoua, M., Fall, M., & Belem, T. (2004). A contribution to understanding the hardening process of cemented pastefill. *Minerals Engineering*, *17*(2): 141–152. https://doi.org/10.1016/j.mineng.2003.10.022.

Bhondayi, C., Moys, M. H., Danha, G., & Fanuchi, D. (2015). A numerical study of the effect of gas distribution profile across the pulp-froth interface on flotation performance. *Powder Technology*, *286*: 22–30. https://doi.org/10.1016/j.powtec.2015.07.042.

Cihangir, F., Ercikdi, B., Kesimal, A., Deveci, H., & Erdemir, F. (2015). Paste backfill of high-sulphide mill tailings using alkali-activated blast furnace slag: Effect of activator nature, concentration and slag properties. *Minerals Engineering*, *83*: 117–127. https://doi.org/10.1016/j.mineng.2015.08.022.

Cui, B., Liu, Y., Feng, G., Bai, J., Du, X., Wang, C., & Wang, H. (2020). Experimental study on the effect of fly ash content in cemented paste backfill on its anti-sulfate erosion. *International Journal of Green Energy*, *17*(12): 730–741. https://doi.org/10.1080/15435075.2020.1791877.

Cui, L., & Fall, M. (2018). Multiphysics Modeling and Simulation of Strength Development and Distribution in Cemented Tailings Backfill Structures. *International Journal of Concrete Structures and Materials*, *12*(1). https://doi.org/10.1186/s40069-018-0250-y.

Cui, L., & Fall, M. (2019). Mathematical modelling of cemented tailings backfill: a review. *International Journal of Mining, Reclamation and Environment*, *33*(6): 389–408. https://doi.org/10.1080/17480930.2018.1453320.

Dong, Q., Liang, B., Jia, L., & Jiang, L. (2019). Effect of sulfide on the long-term strength of lead-zinc tailings cemented paste backfill. *Construction and Building Materials*, *200*: 436–446. https://doi.org/10.1016/j.conbuildmat.2018.12.069.

Ercikdi, B., Cihangir, F., Kesimal, A., Deveci, H., & Alp, I. (2009). Utilization of industrial waste products as pozzolanic material in cemented paste backfill of high sulphide mill tailings. *Journal of Hazardous Materials*, *168*(2–3): 848–856. https://doi.org/10.1016/j.jhazmat.2009.02.100.

Ercikdi, B., Kesimal, A., Cihangir, F., Deveci, H., & Alp, I. (2009). Cemented paste backfill of sulphide-rich tailings: Importance of binder type and dosage. *Cement and Concrete Composites*, *31*(4): 268–274. https://doi.org/10.1016/j.cemconcomp.2009.01.008.

Ethier, M. P., Bussière, B., Aubertin, M., Maqsoud, A., Demers, I., & Broda, S. (2018). In situ evaluation of performance of reclamation measures implemented on abandoned reactive tailings disposal site. *Canadian Geotechnical Journal*, *55*(12): 1742–1755. https://doi.org/10.1139/cgj-2016-0699.

Fall, M., & Benzaazoua, M. (2005). Modeling the effect of sulphate on strength development of paste backfill and binder mixture optimization. *Cement and Concrete Research*, *35*(2): 301–314. https://doi.org/10.1016/j.cemconres.2004.05.020.

Fall, M., Belem, T., Samb, S., & Benzaazoua, M. (2007). Experimental characterization of the stress-strain behaviour of cemented paste backfill in compression. *Journal of Materials Science*, *42*(11): 3914–3922. https://doi.org/10.1007/s10853-006-0403-2.

Fang, K., & Fall, M. (2019). Chemically Induced Changes in the Shear Behaviour of Interface Between Rock and Tailings Backfill Undergoing Cementation. *Rock Mechanics and Rock Engineering*, *52*(9): 3047–3062. https://doi.org/10.1007/s00603-019-01757-0.

Fang, K., Cui, L., & Fall, M. (2020). A coupled chemo-elastic cohesive zone model for backfill-rock interface. *Computers and Geotechnics*, *125*(June): 103666. https://doi.org/10.1016/j.compgeo.2020.103666.

Fu, J. X., Song, W. D., & Tan, Y. Y. (2016). Study on Microstructural Evolution and Strength Growth and Fracture Mechanism of Cemented Paste Backfill. *Advances in Materials Science and Engineering*, *2016*. https://doi.org/10.1155/2016/8792817.

Gallé, C. (2001). Effect of drying on cement-based materials pore structure as identified by mercury intrusion porosimetry - A comparative study between oven-, vacuum-, and freeze-drying. *Cement and Concrete Research*, *31*(10): 1467–1477. https://doi.org/10.1016/S0008-8846(01)00594-4.

Ghirian, A., & Fall, M. (2016). Long-term coupled behaviour of cemented paste backfill in load cell experiments. *Geomechanics and Geoengineering*, *11*(4): 237–251. https://doi.org/10.1080/17486025.2016.1145256.

Guo, S., Fall, M., & Haruna, S. (2020). Interface Shear Behavior of Cementing Underground Mine Backfill. *International Journal of Geomechanics*, *20*(12): 04020230. https://doi.org/10.1061/(asce)gm.1943-5622.0001852.

Hussain A, Pu L, Underwood J. Strain energy release rate for a crack under combined Mode-I and Mode II. Fract. Anal ASTM STP 1974;560:2-28.

Jafari, M., Shahsavari, M., & Grabinsky, M. (2021). Drained Triaxial Compressive Shear Response of Cemented Paste Backfill (CPB). *Rock Mechanics and Rock Engineering*, *54*(6): 3309–3325. https://doi.org/10.1007/s00603-021-02464-5.

Kesimal, A., Yilmaz, E., & Ercikdi, B. (2004). Evaluation of paste backfill mixtures consisting of sulphide-rich mill tailings and varying cement contents. *Cement and Concrete Research*, *34*(10): 1817–1822. https://doi.org/10.1016/j.cemconres.2004.01.018.

Li, H., Liu, Y., Wang, K., Guo, Y., Cui, B., & Yan, R. (2018). *A Summary of Research on the Durability of Cemented Paste Backfill in Mines*. *176*: 258–263. https://doi.org/10.2991/coal-18.2018.47.

Li, W., & Fall, M. (2016). Sulphate effect on the early age strength and self-desiccation of cemented paste backfill. *Construction and Building Materials*, *106*: 296–304. https://doi.org/10.1016/j.conbuildmat.2015.12.124.

Li, W., & Fall, M. (2018). Strength and self-desiccation of slag-cemented paste backfill at early ages: Link to initial sulphate concentration. *Cement and Concrete Composites*, *89*: 160–168. https://doi.org/10.1016/j.cemconcomp.2017.09.019.

Li, X., Snellings, R., & Scrivener, K. L. (2019). Quantification of amorphous siliceous fly ash in hydrated blended cement pastes by X-ray powder diffraction. *Journal of Applied Crystallography*, *52*: 1358–1370. https://doi.org/10.1107/S1600576719013955.

Libos, I. L. S., & Cui, L. (2020). Effects of curing time, cement content, and saturation state on mode-I fracture toughness of cemented paste backfill. *Engineering Fracture Mechanics*, *235*(May), 107174. https://doi.org/10.1016/j.engfracmech.2020.107174.

Libos, I. L. S., & Cui, L. (2020). Mechanical properties and behavior of early-age fiber-reinforced cemented paste backfill. *International Conference on Civil, Structural and Transportation Engineering*, *201406430051*: 193-1-193–196. https://doi.org/10.11159/iccste20.193.

Liu, Y., Li, H., & Wu, H. (2019). Experimental Study on Mechanical Properties of Cemented Paste Backfill under Temperature-Chemical Coupling Conditions. *Advances in Materials Science and Engineering*, *2019*. https://doi.org/10.1155/2019/9754790.

Ma, H. (2014). Mercury intrusion porosimetry in concrete technology: Tips in measurement, pore structure parameter acquisition and application. *Journal of Porous Materials*, *21*(2): 207–215. https://doi.org/10.1007/s10934-013-9765-4.

Nasir, O., & Fall, M. (2008). Shear behaviour of cemented pastefill-rock interfaces. *Engineering Geology*, *101*(3–4): 146–153. https://doi.org/10.1016/j.enggeo.2008.04.010.

Orejarena, L., & Fall, M. (2010) Artificial Neural Network Modelling of the Coupled Effect of Sulphate and temperature on the Strength of Cemented Paste Backfill. NRC Research press web site. cjce.nrc.ca.

Pokharel, M., & Fall, M. (2013). Combined influence of sulphate and temperature on the saturated hydraulic conductivity of hardened cemented paste backfill. *Cement and Concrete Composites*, *38*: 21–28. https://doi.org/10.1016/j.cemconcomp.2013.03.015.

Pycnometer, W., Barrel, S. (2009). Standard Test Methods for Laboratory Determination of Density (Unit Weight) of Soil.1–7. https://doi.org/10.1520/D7263-21.1.2

Rong, H., Zhou, M., & Hou, H. (2017). Pore structure evolution and its effect on strength development of sulfate-containing cemented paste backfill. *Minerals*, *7*(1). https://doi.org/10.3390/min7010008.

Sahinoglu, E. (2018). Cleaning of high pyritic sulfur fine coal via flotation. *Advanced Powder Technology*, *29*(7): 1703–1712. https://doi.org/10.1016/j.apt.2018.04.005.

Schöllmann, M., Richard, H. A., Kullmer, G., & Fulland, M. (2002). A new criterion for the prediction of crack development. *International Journal of Fracture*, *117*, 129–141.

Shaikhon, O. (2015). *The Effect of Chloride and Sulfate Ions on the Resistivity of Concrete*. *23*(July): 139–146. http://linkinghub.elsevier.com/retrieve/pii/000888469390144X.

Sih, G. C. (1974). Strain-energy-density factor applied to mixed mode crack problems. *International Journal of Fracture*, *10*(3), 305–321. https://doi.org/10.1007/BF00035493

Vyazmensky, A. (2008). Numerical modeling of surface subsidence associated with block cave mining using a FEM/DEM approach.

Wang, Z. Z., Wu, A. X., & Wang, H. J. (2020). A Strength Design Method of Cemented Backfill with a High Aspect Ratio. *Advances in Civil Engineering*, *2020*. https://doi.org/10.1155/2020/7159208.

Xiu, Z., Wang, S., Ji, Y., Wang, F., Ren, F., & Nguyen, V. T. (2021). Loading rate effect on the uniaxial compressive strength (UCS) behavior of cemented paste backfill (CPB). *Construction and Building Materials*, *271*: 121526. https://doi.org/10.1016/j.conbuildmat.2020.121526.

Xu, X., Wu, W., & Xu, W. (2020). Sulfate-dependent shear behavior of cementing fiber-reinforced tailings and rock. *Minerals*, *10*(11): 1–22. https://doi.org/10.3390/min10111032.

Xu, X., Wu, W., & Xu, W. (2020). Sulfate-dependent shear behavior of cementing fiber-reinforced tailings and rock. *Minerals*, *10*(11): 1–22. https://doi.org/10.3390/min10111032.

Yan, B., Zhu, W., Hou, C., Yu, Y., & Guan, K. (2020). Effects of coupled sulphate and temperature on internal strain and strength evolution of cemented paste backfill at early age. *Construction and Building Materials*, *230*, 116937. https://doi.org/10.1016/j.conbuildmat.2019.116937.

Yilmaz, E. (2018). Stope depth effect on field behaviour and performance of cemented paste backfills. *International Journal of Mining, Reclamation and Environment*, *32*(4): 273–296. https://doi.org/10.1080/17480930.2017.1285858.